ABSTRACT

HAUGH, JANINE M. Mathematical Modeling of Cartilage Regeneration in Cell-Seeded Scaffolds. (Under the direction of Dr. Mansoor Haider).

Articular cartilage is the hydrated orthopaedic soft tissue lining the surfaces of bones in diarthrodial joints such as the knee, shoulder and hip. Cartilage degeneration due to osteoarthritis or injury can lead to osteochondral defects in the cartilage layer. Tissue engineering applications based on chondrocyte-biomaterial systems have the potential to regenerate cartilage in a controlled environment, but the optimal combination of diverse factors required to successfully regenerate articular cartilage is not known. Two approaches to mathematical modeling of articular cartilage regeneration in cell-seeded scaffold materials are presented.

First, a spatio-temporal PDE model that combines a level set approach with a system of reaction-diffusion equations is developed for modeling the local environment of a single chondrocyte in a scaffold material. This approach accounts for spatial variability in hydrogel scaffold density and degradation, and the associated changes in diffusivities through the scaffold and regenerated extracellular matrix (ECM). The diffusive quantities considered are nutrients and newly synthesized matrix, and the creation of linked ECM is represented by an evolving gel-tissue interface. The model is nondimensionalized and solutions are computed numerically via finite difference methods. A parametric analysis is performed to quantify the effects of model parameters on a regeneration time for a targeted volume of regenerated ECM. A possible model simplification is also presented, where the nutrient concentration is assumed to remain constant.

Second, a phenomenological ODE model that differentiates the ECM into its collagen and glycosaminoglycan (GAG) constituents, as well as the linked and unlinked components of each is developed. This model is calibrated using experimental data by way of a nonlinear least squares approach, and a parametric analysis to quantify the effects of model parameters on a regeneration time for a targeted value of linked ECM is performed. For both modeling approaches, results focus on characterizing the relationships between scaffold design and regeneration times for accumulation of cell-synthesized ECM to aid in cartilage regeneration optimization in tissue engineering applications for chondrocyte-biomaterial systems.

Mathematical Modeling of Cartilage Regeneration in Cell-Seeded Scaffolds

by
Janine M. Haugh

A dissertation submitted to the Graduate Faculty of
North Carolina State University
in partial fullfillment of the
requirements for the Degree of
Doctor of Philosophy

Applied Mathematics

Raleigh, North Carolina

2010

APPROVED BY:

_____   _____
Dr. Sharon Lubkin   Dr. Farshid Guilak

_____   _____
Dr. Mansoor Haider   Dr. Ralph Smith
Chair of Advisory Committee

DEDICATION

I'd like to dedicate this to my father:

Thomas Haugh

9/11/1956 – 6/3/2010

The world won't be the same without you, but I promise to carry on your love for life and passion for learning and teaching as best I can. I love you and miss you more than I can possibly express on this page.

BIOGRAPHY

Janine Marie Haugh was born in Manchester, NH on August 13, 1983. She is the oldest of three daughters of Thomas and Terry Haugh. She attended Main Dunstable Elementary School in Nashua, NH through first grade. When she was six years old, her family moved to Amherst, NH where she attended Wilkins Elementary School, Amherst Middle School, and Souhegan High School, from which she graduated in 2001. She graduated Summa Cum Laude from the University of New Hampshire in Durham, NH with a Bachelor of Science in Mathematics and a Minor in Physics in May 2005.

After her college graduation, Janine moved to the southern city of Raleigh, NC in order to attend North Carolina State University. She earned her Masters of Science in Applied Mathematics in 2007 and her Doctor of Philosophy degree in Applied Mathematics in the Summer of 2010 under the guidance of Dr. Mansoor Haider. After over two decades of being a student, Janine has accepted a position at the University of North Carolina Asheville where she will begin the next chapter of her life, as an Assistant Professor of Mathematics, in August 2010.

ACKNOWLEDGMENTS

First of all, I'd like to thank my family. My parents, Tom and Terry Haugh, and my sisters, Angela and Christie, who have always been there for me whenever and however I needed them to be. I'd also like to thank David Mirfin, Jr., for understanding and supporting me every single day. Their love and support means everything to me.

I'd like to thank to my high school teachers Viet and Amy Pham, who first planted the ideas of going on to graduate school and teaching at the college level in my head nearly a decade ago. I am forever indebted to two of my college math professors, Gertrud Kraut and Kelly Black, without whom I truly believe I would not be where I am today (both pedagogically and geographically). I'd also like to thank my freshman physics professor, Bob Simpson, for helping me decide to change my major to mathematics, Rita Hibschweiller and Dawn Meredith, who offered me valuable guidance and support throughout college, and my REU advisor, Kurt Bryan, for giving me my first taste of mathematics research.

While at NCSU I have formed some great memories with a wonderful group of friends, so I owe thanks to Leslie Kurtz, Ryan Therkelsen, Mike Allocca, Louis Levy, Tom Wears, Nick Giffen, Kristen Stagg, Susan Crook, Catherine Buell, Jon Dunbar, Brandy Benedict, and many others. I'm also thankful for my "study dates" with Marybeth Brey, Anita McCulloch, and Meredith Adams, and the constant moral support they provided for me during my last semester as a student. I'd also like to thank Sarah Ann Stewart and the rest of the CaMeW crew for all of their guidance, and for encouraging me to trust my instincts.

Many of the faculty and staff at NCSU have made an impact on me during my time here, but I'd particularly like to thank my advisor, Mansoor Haider, and my committee members, Ralph Smith, Sharon Lubkin, and Farshid Guilak, for taking the time to help me get to this point in my education, and especially for being so understanding and accommodating during the last month or so when I've had to deal with the sudden loss of my father. I'd also like to thank Steve Campbell for all of

the fun stories and countless pep talks, Maxine Atkinson for giving me the amazing opportunity to teach with the FYI program and forever altering my teaching style for the better, Jane Griffiths for helping me realize that I'm much stronger than I ever gave myself credit for, and Michael Shearer for letting me tag along at conferences. I also owe thanks to the National Science Foundation for supporting me for the last two years through the Research Training Grant on Mathematics of Materials (NSF-DMS-0636590).

Lastly, I want to thank all of the students I've had the great fortune to be able to teach and tutor over the years. Whenever I've been discouraged or frustrated with school, research, or life in general, it has been teaching them that has kept me grounded and given me direction. I have learned as much from them as I hope they have learned from me, and I hope that never changes.

Thanks again, everyone. I couldn't have done this alone.

TABLE OF CONTENTS

LIST OF TABLES

LIST OF FIGURES

Chapter 1

Introduction and Background

1.1   Articular Cartilage

Articular cartilage is a soft, hydrated connective tissue which lines the surfaces of bones in diarthrodial joints such as knees (Figure 1.1(a)), hips, and shoulders. The functional role of cartilage is to provide load support, energy dissipation, and lubrication within these joints [33]. It is a multiphasic tissue that is comprised of roughly 80% water (by volume) saturating a solid extracellular matrix (ECM), and is able to withstand high compressive stresses over the course of several decades [19]. The tissue is avascular (no blood vessels), aneural (no nerve endings), and has a limited capacity for self-repair and growth [33]. Cartilage is interspersed with cells, called chondrocytes, that are sparsely distributed throughout the tissue's extracellular matrix (Figure 1.1(b)) [4].

1.1.1   Chondrocytes

Chondrocytes occupy between roughly 1-10% of the mixture volume of articular cartilage, but are crucial to maintaining the overall health of the joint. These unique cells are responsible for regulating homeostasis in the tissue and repairing the ECM constituents when alterations are detected in the local extracellular environment [34]. For example, in cell-biomaterial systems it has been observed that the rate for cellular

biosynthesis of ECM constituents slows down as ECM accumulation progresses [5, 11].

1.1.2 Extracellular Matrix

The extracellular environment in articular cartilage can be viewed as a biphasic (fluid-solid) continuum mixture that is comprised mostly of interstitial fluid with dissolved ions ($\approx$75-80% by wet weight). The remaining (solid) phase consists of a cross-linked network of collagen fibers (mostly type II, $\approx$60% by dry weight) and proteoglycan macromolecules ($\approx$25-35% by dry weight) (Figure 1.2) that give rise to a net negative fixed charge density in the tissue [4].

The ECM contributes to load support though a combination of strain in the solid phase and pressurization of the interstitial fluid. The ECM also protects the chondrocytes from damage due to the effects of joint loading, in part, via a specialized ECM region called the pericellular matrix that encapsulates these cells, individually or in small groups [19]. Additionally, the ECM can regulate the behavior of the chondrocytes through binding of ECM receptors, and binding and release of soluble mediators and growth factors like transforming growth factor (TGF) β [36].

1.2 Cartilage Damage

Each year, millions of Americans experience the debilitating effects of articular cartilage damage caused by trauma, injury, and degenerative diseases such as osteoarthritis. In particular, osteoarthritis has symptoms such as joint pain and restriction of motion that significantly impact quality of life [4]. Aging can cause degradation in the composition of extracellular matrix and chondrocyte biosynthetic activity, and a decrease in proteoglycan density. As a result, a loss of tissue structure and mechanical integrity has been observed in diarthrodial joints. The risk of osteoarthritis is said to greatly increase beginning at age 40 [17] and affects about 70% of people over the age of 65 [18]. Repetitive high impact movement and loading in certain sports can result in injury, and continuing these activities with undiagnosed injury also increases

risk of degenerative diseases [4].

Osteoarthritis involves all of the tissues that form the synovial joint, but most severely affects the articular cartilage. A decrease in proteoglycan concentration and aggregation causes a decrease in tissue stiffness. Water content increases due to increased permeability, further decreasing tissue resiliency. The load on the collagen fibrils and proteoglycans increases, and chondrocytes could be injured as a result. As the disease progresses, the cartilage begins to erode and deteriorate beyond the point of self-repair (Figure 1.3) [4].
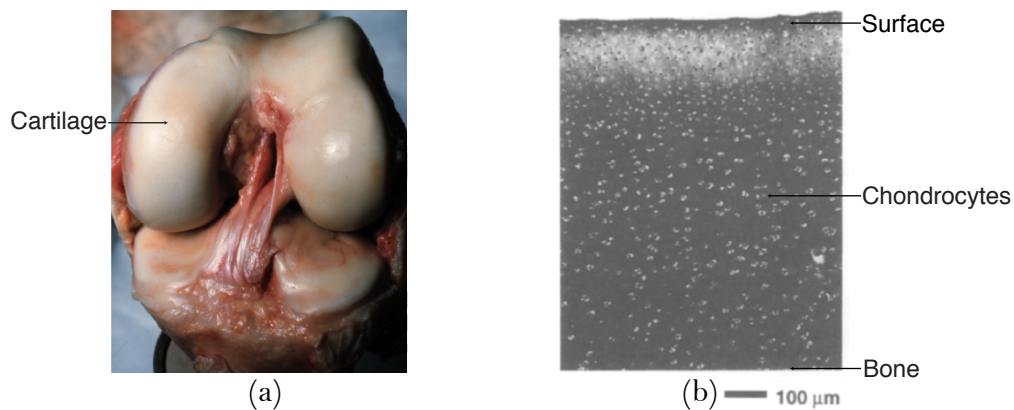
Figure 1.1: (a) Articular cartilage is a translucent orthopaedic soft tissue that lines the surfaces of bones in diarthrodial joints, such as the knee. (b) Cross-section of a layer of articular cartilage, indicating the presence of sparsely distributed cells, called chondrocytes, which monitor and maintain the extracellular matrix. (Reprinted from Osteoarthritis and Cartilage, 2/2, Farshid Guilak, B. Christoph Meyer, Anthony Ratcliffe and Van C. Mow, The effects of matrix compression on proteoglycan metabolism in articular cartilage explants, 91-101, Copyright (1994), with permission from Elsevier.)
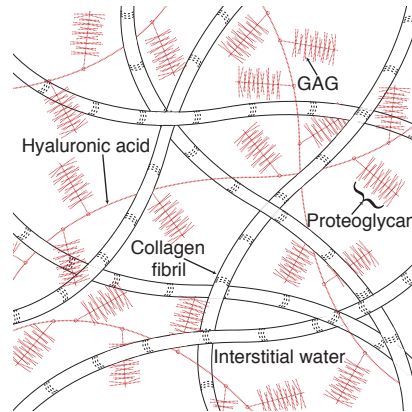
Figure 1.2: The extracellular matrix of articular cartilage is a cross-linked network of collagen and proteoglycans, and is saturated with interstitial fluid containing water and dissolved ions.

(a)	(b)	(c)

Normal	Early Disease	Late Disease
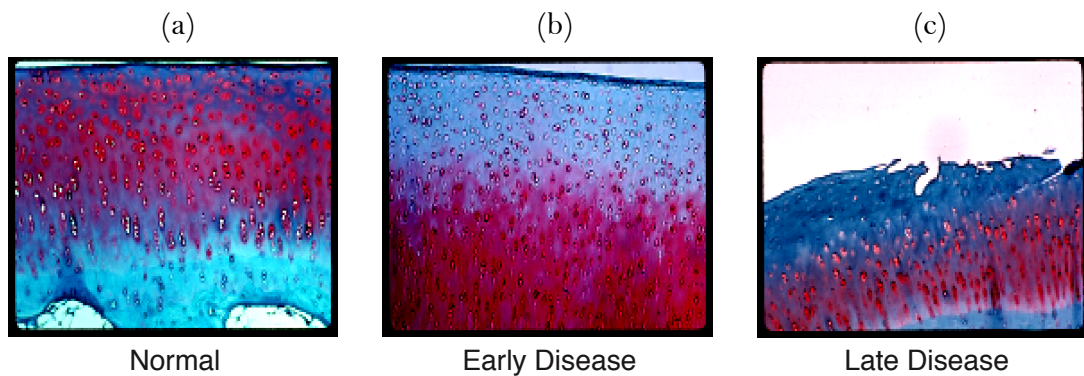
Figure 1.3: (a) Healthy articular cartilage in which the red-purple staining indicates the presence of proteoglycans. (b) In the early stages of osteoarthritis, proteoglycan content decreases and initiates structural degradation of the extracellular matrix. (c) In later stages of osteoarthritis, the tissue becomes less resilient and degrades beyond a point where is has the ability to repair itself. (Photos courtesy of Dr. Lori Setton, Duke University, Cartilage Mechanics and Tissue Engineering Laboratory.

1.3   Tissue Engineering for Cartilage Regeneration

The debilitating effects of osteoarthritis affect a large portion of the population. Consequently, research on tissue engineering for cartilage repair and regeneration has seen great interest in the past few decades. Developing tissue engineering strategies that preserve the unique and complex properties of native articular cartilage proves to be a difficult task for biomedical researchers [18]. According to O'Driscoll [25], the treatment options for damaged cartilage include "the four r's": restoration, replacement, relief, and resection. Cartilage regeneration, which falls under the first category of restoration, has seen many developments in recent years and will be the focus of this work.

Chondrocytes can be cultured or seeded into biodegradable and biocompatible polymer or hydrogel scaffolds to aid in cartilage regeneration. The scaffolds provide the needed support and framework for the cells to proliferate and/or recognize and initiate the process of repair or regeneration of ECM. As the synthesis and accumulation of ECM constituents progress, the scaffold slowly degrades [12]. To be successful, the new tissue must be able to integrate, both structurally and functionally, with the surrounding cartilage either by grafting of engineered tissue *in vitro* into defect sites, or by way of tissue engineering strategies that can be applied *in situ* within the defect regions. Many types of scaffolds are being studied for this purpose, including collagen-based, polyglycolic acid (PGA), polylactic acid (PLA), fibrin, alginate, agarose, and polyethlene oxide [13].

In Figure 1.4, an example of an *in situ* cartilage regeneration experiment is shown. Nettles et al. [21, 22] used an injectable crosslinkable elastin-like polypeptide (ELP) gel to fill osteochondral defects in goats (a). Chondrocytes were mixed with ELP solution and cultured into gelatinous cylindrical molds (b). Via customizable design of the ELP polymer, this solution can be tailored to exhibit a phase transition from a liquid to a gelatinous solid phase near physiological temperature (c). This tissue engineering strategy allows the gelling to occur *in situ* to properly fill the defect with a stable and well-integrated scaffold (d). While many positive results were

observed with this methodology, more work is needed to optimize the ELP design and formulation process to, for example, slow down the degradation rate of the scaffold [21, 22].

As Nettles et al. [21, 22] observed, the development of tissue engineering strategies for cartilage regeneration depends on a diverse array of factors that require detailed analysis and optimization to achieve targeted functional outcomes in the engineered tissue. In applications involving cell-seeded scaffolds, there are numerous factors that can be varied to alter outcomes. Some experiments expose the cells to a highly dynamic environment, such as those in rotating bioreactors. Others are more static in their nature and involve culturing or seeding cells into a scaffold material and allowing the cell-biomaterial system to evolve under sustained exposure to nutrients and/or growth factors such as TGF-β [28, 36]. The scaffolds themselves can be made of many different materials with numerous porosities or cross-linking densities, and they will not all degrade at the same rate. Chondrocyte seeding densities, rates of cell proliferation, and effects due to osmotic loading are all examples of factors that can play a role in affecting the resulting functional outcomes. Such outcomes also depend on transport and utilization of nutrients, cellular biosynthesis of ECM constituents, and the associated diffusivities of these components of the system. Given the large number of parameters and the diverse set of interacting mechanisms at play, mathematical models to quantify the importance of these mechanisms and predict the outcome of experiments could prove to be extremely beneficial for eliminating (or minimizing) trial and error and optimizing the scaffold design process [32].
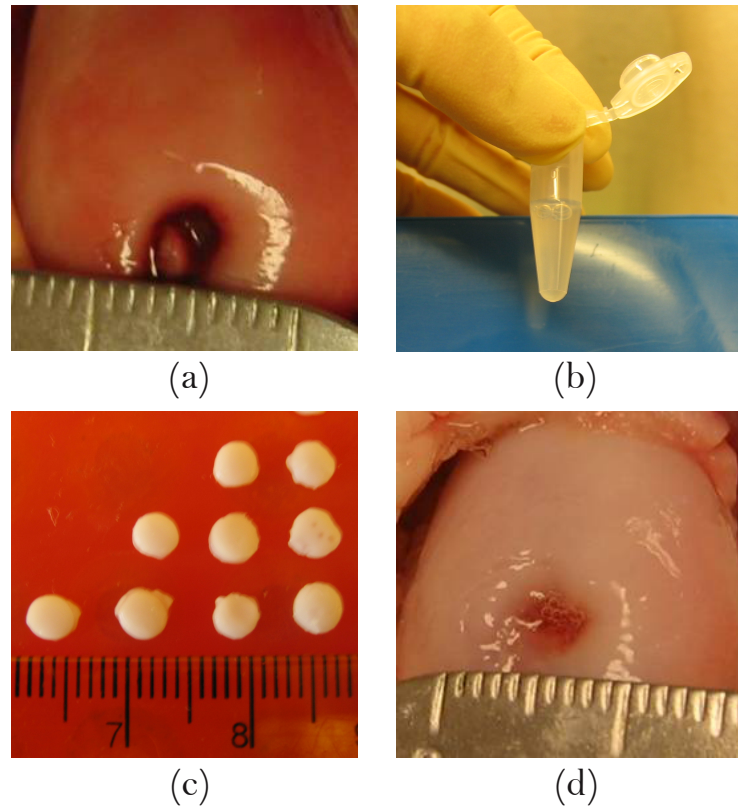
Figure 1.4: (a) An osteochondral defect prior to repair. (b) Chondrocytes and elastin-like polypeptide (ELP) are mixed into a solution. (c) Tailored design of the ELPs enable a phase transition forming a gel near physiological temperatures. (d) An osteochondral defect filled with the cell-biomaterial scaffold based on the combination of ELP hydrogels with articular chondrocytes. (Reprinted from Tissue Engineering Part A, 15/8, Dana L. Nettles, Ashutosh Cilkoti, and Lori A. Setton, Early metabolite levels predict long-term matrix accumulation for chondrocytes in elastin-like polypeptide biopolymer scaffolds, 2113-2121, Copyright (2009), with permission from Mary Ann Liebert, Inc.)

1.4   Models for Cartilage Regeneration

1.4.1   Statio-Temporal (PDE) Models

Many of the mathematical models that have been developed for cartilage regeneration applications are based on the use of partial differential equations [1, 2, 3, 6, 7, 8, 9, 14, 23, 24, 27, 31, 35]. An advantage of these models is their formulation in terms of physically meaningful parameters, many of which can be determined from associated experiments. For example, mechanisms such as diffusion are modeled explicitly, and diffusivities for various solute types and sizes are known or can be measured [15, 16]. Structural properties of cartilage ECM vary spatially, both with respect to depth within the cartilage layer, and in proximity to the chondrocytes. Biphasic continuum variables such as stress, strain, and osmotic pressure vary spatially as well [19]. Any subset of these mechanisms and variables can be used to develop models of cartilage regeneration based on the specific mechanisms or interactions of interest.

Bachrach et al. [3] used a biphasic model to study how mechanical changes in the environment of a chondrocyte affect proteoglycan synthesis. Their model was able to analyze how stress, strain, pressure, and flow in the surrounding tissue evolved with cellular biosynthesis of ECM proteoglycans. Galban and Locke [7, 8, 9] took a different approach and developed models for chondrocyte growth and nutrient consumption. Reaction-diffusion models were employed, and cell growth was determined by a moving boundary. They later extended this model to use volume-averaging methods to study cell growth and effective diffusion profiles.

DiMicco and Sah [6] developed a one-dimensional continuum model to describe the relationships between matrix formation, binding, degradation, and diffusion by separating the matrix into three categories: soluble, bound, and degraded. Parameters were interpreted from the literature, and the resulting steady-state solution was spatially averaged for comparison with a single compartment model.

Obradovic et al. [24] isolated chondrocytes from bovine calf articular cartilage, seeded them onto fibrous, biodegradable PGA scaffolds, and cultured them in ro-

tating bioreactors. They used reaction-diffusion equations and Michaelis-Menten kinetics to model oxygen transport and consumption, and used similar equations to model GAG production, degradation, transport, and deposition within a cylindrical construct. Nikolaev et al. [23] later extended this work under the assumption that newly synthesized proteoglycan, or "unbound GAG", diffuses freely and is considered separately from "bound GAG", similar to DiMicco and Sah [6]. Tissue growth in this model was quantified by the amount of bound GAG accumulation, or proteoglycan aggregation.

Sengers et al. [31] focused on nutrient utilization of chondrocytes by developing models for oxygen, glucose, and lactate diffusion and consumption. Pisu et al. [27] employed reaction-diffusion equations to model oxygen, GAG, and collagen concentrations in a static system, which they validated against data for multiple types of scaffolds, including PGA, PGA/poly L-lactic acid (PLLA), and collagen sponge. Albro et al. [1] investigated the effects of osmotic loading on spherical gels in order to draw conclusions about chondrocyte response. Kohles, Wilson, and Bonassar [14] employed a composite spheres model to determine biomechanical and biochemical behavior at the cellular level for chondrocytes seeded in PGA/PLLA scaffolds.

More recently, Ateshian et al. [2] developed a continuum model which addresses cell division, effects of osmotic loading, tissue growth, fixed charge density, cell volume regulation, and other effects within a continuum mixture theory framework. Also, Trewanek et al. [35] developed a continuum model for soluble matrix components, bound matrix components, and remaining scaffold material.

1.4.2 Phenomenological (ODE) Models

A challenge in application of the aforementioned PDE models is the difficulty in obtaining spatial data in cell-biomaterial systems. In addition, cartilage regeneration occurs on time scales that span many weeks to several months. As a result, many experimentalists have measured only scalar system variables such as scaffold or collagen dry mass at a small number of time points. Consequently, a mathematical modeling

approach based on ordinary differential equations (ODEs) appears to be a natural choice for analysis of dynamic evolution of these system variables.

However, to date, significantly less work has been done with ordinary differential equation models. Wilson et al. [38] developed models for scaffold degradation, ECM production (differentiating between GAG and collagen), and the resulting total mass of the construct. These models were then fitted to and validated against multiple sets of data. Although the models were incredibly simple, they did fit reasonably well to the data. Saha et al. [30] then extended this model to include the impact of growth factors using stochastic methods. Vunjak-Novakovic et al. [37] used a dynamic model to investigate ways to optimize seeding conditions.

In the chapters that follow, both the PDE and ODE approaches for modeling cartilage regeneration in cell-seeded scaffold materials will be examined. First, a PDE model that combines a level set approach with a system of reaction-diffusion equations is developed for the local environment of a single chondrocyte. This approach accounts for spatial variability in hydrogel scaffold density and degradation, and the associated changes in diffusivities through the scaffold and regenerated ECM. Second, a phenomenological ODE model extending the work of Wilson et al. [38] is developed. This model differentiates the ECM into its collagen and GAG constituents, and also into the linked and unlinked components of each. For both approaches, results focus on characterizing the relationships between scaffold design and regeneration times for accumulation of cell-synthesized ECM to aid in cartilage regeneration optimization in tissue engineering applications for chondrocyte-biomaterial systems.

Chapter 2

Reaction-Diffusion Model: Development and Methods

2.1 Introduction

To gain a better understanding of the importance of spatial effects on cartilage regeneration in a cell-seeded scaffold material, reaction-diffusion models are often used to describe the evolving tissue construct (see Section 1.4.1). Within the context of these models, two approaches have been used. In one approach, employed in several previously published studies, macroscopic reaction-diffusion models were developed for an entire cylindrical construct [23, 24, 27]. An alternate approach by Kohles et al. [14] focuses on modeling tissue regeneration in the local environment of a single chondrocyte seeded in a nutrient-rich hydrogel scaffold material, as seen in Figure 2.1.

The current study employs this second approach, and captures the interactions among extracellular matrix (ECM) synthesis, accumulation, and diffusive transport phenomena in a manner that also accounts for cell shape and the ratio of initial cell to scaffold volume. It is assumed that this process is radially symmetric within a spherical domain, and the ECM is synthesized, diffuses, and accumulates uniformly around the periphery of the chondrocyte. Following the assumptions of DiMicco et

al. [6], the unlinked matrix is synthesized inside the cell and diffuses freely until it binds with the scaffold, eventually replacing the hydrogel. To simplify the model, the process by which the synthesized matrix interacts with hydrogel to form linked ECM is represented as an advancing interfacial region (Figure 2.2). Specifically, this interface represents the evolving boundary between the newly formed linked ECM domain and the degrading hydrogel region. Level set and phase field modeling techniques are employed to capture the motion of this advancing region.
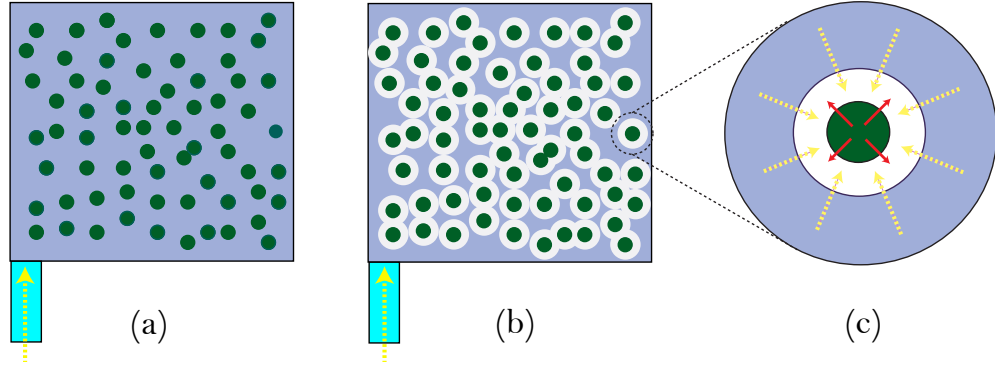
Figure 2.1: (a) A nutrient-rich hydrogel (light blue) is seeded with sparsely distributed chondrocytes (green). (b) Over time, the chondrocytes absorb and utilize nutrients (yellow) and synthesis new ECM (white). (c) The model described in this chapter focuses on the complex interactions in the local environment of a single chondrocyte.

2.2 Model Development

2.2.1 Introduction

There are four variables being considered in this model: nutrient concentration, unlinked matrix concentration, hydrogel density, and the location of the gel-tissue interfacial region. Note that the advancing interface location also, effectively, determines the amount of linked ECM volume that has been regenerated. The nutrients and unlinked matrix are diffusing molecules, and are thus modeled via reaction-diffusion equations. As a general strategy, assume that $X = X(r,t)$ is a diffusing molecule in a cell-seeded hydrogel. It can be said that

$$\frac{\partial X}{\partial t} \;=\; \nabla \cdot (D_X(r)\nabla X) + f\left(X, Y\right), \quad 0 < r < R, \; t > 0 \qquad (2.1)$$

where $D_X(r)$ is the diffusivity of X through conditions at point r in space, and $Y = Y(r,t)$ could represent any other relevant variables. Also note that R is the outer boundary of the domain for a single chondrocyte (as in Figure 2.2(b)), and it is assumed that $R \gg a$, where a is the cell radius, since chondrocytes are sparsely distributed in articular cartilage ECM. Also, note that the diffusivity can vary spatially. This concept will be discussed in greater detail in later sections. The function $f\left(X, Y\right)$ could take a number of forms, and represents a reaction or interaction between X and Y that, locally, alters the amount of one or both quantities. If X is a non-diffusing variable, such as the hydrogel, the equation would simply take on the form

$$\frac{\partial X}{\partial t} \;=\; f\left(X, Y\right), \quad 0 < r < R, \; t > 0 \qquad (2.2)$$

The evolving nature of the ECM region is modeled using a different method, which will be described in more detail in Section 2.2.4.
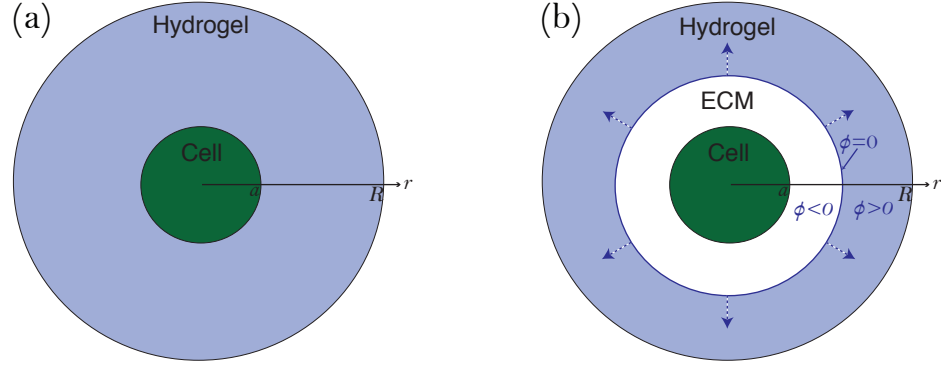
Figure 2.2: An illustration of the local cartilage regeneration model is shown. (a) Chondrocytes are seeded in a nutrient-rich hydrogel scaffold at $t = 0$. (b) As time progresses, the cell utilizes nutrients to synthesize unlinked matrix that forms a linked ECM region outside the cell. Note that $\phi = 0$ is the location of the evolving gel-tissue interfacial region, with $\phi < 0$ denoting the regenerated tissue, and $\phi > 0$ denoting the hydrogel region.

2.2.2   Intracellular Region

Since hydrogel scaffolds are typically rich in nutrients, the hydrogel is initially assumed to have nutrient concentration N_H, which can be greater than the concentration associated with healthy mature cartilage at homeostasis, N_*. It is assumed that excess nutrients enter the chondrocyte by way of diffusion, where they are utilized for synthesis of unlinked matrix proteins (Figure 2.3). These matrix proteins assemble and accumulate inside the cell (i.e. $0 < r < a$), and then re-enter the extracellular region by way of diffusion. To capture the chondrocyte's regulatory feedback mechanism, it is assumed that synthesis of these matrix molecules continues as long as the stiffness of the evolving extracellular region is less than a specified stiffness for mature native cartilage. Based on these assumptions, the following model for nutrient and unlinked matrix concentration, $N = N(r,t)$ and $M = M(r,t)$ respectively, is

formulated for the intracellular region

$$\frac{\partial N}{\partial t} = D_N^{(1)} \nabla^2 N - k_N \left(N - N_*\right), \qquad\qquad 0 < r < a,\ t > 0 \qquad (2.3)$$

$$\frac{\partial M}{\partial t} = D_M^{(1)} \nabla^2 M + k_M \left(E_{ECM} - E_{agg}(t)\right) \left(N - N_*\right), \quad 0 < r < a,\ t > 0. \qquad (2.4)$$

In (2.3) and (2.4), $D_N^{(1)}$ and $D_M^{(1)}$ are diffusivities of the nutrient and unlinked matrix inside the cell, and k_N and k_M are physiological parameters representing nutrient absorption and matrix synthesis rates, respectively. The second term on the right hand side of (2.3) accounts for utilization of nutrients required for synthesis of unlinked matrix. Similarly, the second term on the right hand side of (2.4) models the mechanism by which greater nutrient availability increases cellular synthesis of unlinked matrix. It is also assumed that the stiffness of the evolving extracellular gel-tissue aggregate is determined by the stiffness of the remaining hydrogel and the newly linked ECM. This results in the relation

$$
\begin{aligned}
E_{ECM} - E_{agg}(t) \ &= \ E_{ECM} - \left(\frac{V_{ECM}(t)}{V_H(0)} E_{ECM} + \frac{V_H(t)}{V_H(0)} E_H(t)\right) \qquad (2.5) \\
&= \ \left(E_{ECM} - E_H(t)\right)\left(1 - \frac{V_{ECM}(t)}{V_H(0)}\right)
\end{aligned}
$$

where $V_{ECM}(t)$ is the volume of the regenerated ECM region at time t, $V_H(t)$ is the volume of the remaining hydrogel, $V_H(0)$ is the initial hydrogel volume, E_{ECM} is the stiffness of healthy native cartilage, and $E_H(t)$ is the average stiffness of the remaining hydrogel. In deriving the simplified form of (2.5), the relation

$$V(t) \ = \ V_H(0) = V_H(t) + V_{ECM}(t) \qquad (2.6)$$

was employed, where the volume of the extracellular region $V(t)$ is constant. It should also be noted that hydrogel is non-diffusing, and thus hydrogel density $H = H(r,t)$ within the cell is defined to be exactly

$$H(r,t) = 0, \qquad 0 < r < a,\ t > 0. \qquad (2.7)$$
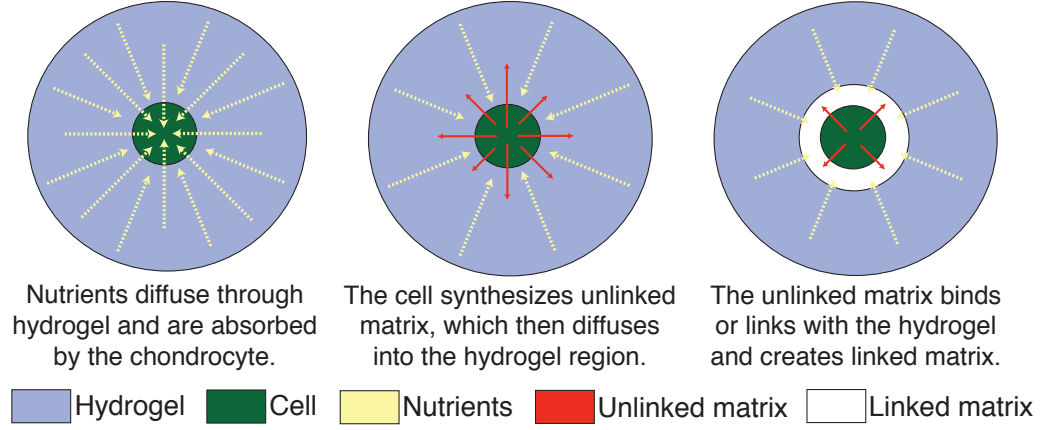
Figure 2.3: An illustration of the primary variables in the local cartilage regeneration model is shown. Nutrients, $N(r,t)$, are absorbed by the cell and utilized in the synthesis of unlinked matrix proteins, $M(r,t)$. As these matrix proteins accumulate, they diffuse back into the hydrogel, $H(r,t)$, where they cross-link to create new ECM (linked matrix). The interfacial region between the linked ECM and the hydrogel is tracked using a level set function, $\phi(r,t)$.

2.2.3   Extracellular Region

The rates of nutrient and unlinked matrix diffusion in the region surrounding the chondrocyte are modeled to vary as the extracellular region transitions from hydrogel to linked ECM. Since the location of the advancing linked ECM region will be captured by a level set function $\phi = \phi(r,t)$, the evolving extracellular diffusivities are represented as functions $D_N(H, \phi)$ and $D_M(H, \phi)$ [15]. While, initially, there is no unlinked matrix present in the system, as these molecules are synthesized and diffuse out of the cell, they begin to link and bind with the hydrogel scaffold, at which point they become stationary (non-diffusing). The rate at which these interactions remove unlinked matrix and hydrogel from the system are captured via the parameters c_M and c_H, respectively. It should also be noted that the hydrogel can exhibit additional degradation, due to natural or external factors, that is independent of interactions with unlinked ECM and occurs at a rate m_H. Based on these assumptions, the

following model is formulated for the extracellular region

$$\frac{\partial N}{\partial t} = \nabla \cdot (D_N(H,\phi)\nabla N), \qquad\qquad a < r < R, \ t > 0, \qquad\qquad (2.8)$$

$$\frac{\partial M}{\partial t} = \nabla \cdot (D_M(H,\phi)\nabla M) - c_M MH, \qquad a < r < R, \ t > 0, \qquad\qquad (2.9)$$

$$\frac{\partial H}{\partial t} = -c_H MH - m_H H, \qquad\qquad a < r < R, \ t > 0. \qquad\qquad (2.10)$$

2.2.4 Level Set Model for ECM Regeneration

In order to measure the progression of cartilage regeneration in a cell-seeded scaffold, a level set approach is used to track the accumulation of a linked ECM region by modeling the location of the ECM-hydrogel interface. It is assumed that this interface, represented by the level set $\phi(r,t) = 0$, propagates in the normal direction with velocity $\vec{V}$ [26]. The region $\phi > 0$ lies ahead of the advancing interface and represents the hydrogel region that does not yet contain any linked ECM. Similarly, the region $\phi < 0$ lies behind the interface and contains linked ECM and hydrogel that, together, can alter diffusivities of the nutrients and unlinked matrix. Interface movement can be represented by

$$\frac{\partial \phi}{\partial t} + \vec{V} \cdot \nabla \phi = 0, \quad \text{where} \quad \vec{V} = F\vec{n} = F\frac{\nabla\phi}{|\nabla\phi|}. \qquad\qquad (2.11)$$

It is assumed that linked matrix accumulation depends on the product of unlinked matrix and hydrogel concentrations, with a linking rate k. A cellular regulatory feedback mechanism (expressed, in this case, in terms of tissue stiffness as in (2.4)), is also included so that linking ceases when a target extracellular stiffness is reached. Based on these assumptions, the level set model is

$$\frac{\partial \phi}{\partial t} + F\,|\nabla\phi| = 0, \quad \text{where} \quad F = kMH\left(E_{ECM} - E_{agg}(t)\right), \quad a < r < R, \ t > 0.$$

$$(2.12)$$

As stated previously, diffusivity outside of the chondrocyte is dependent on the amount of hydrogel present, and also differs between the ECM and hydrogel regions. Assume that the diffusivity of a quantity i (i.e. N or M) through native mature

cartilage ECM is $D_i^{(2)}$, and its diffusivity through the non-degraded hydrogel is $D_i^{(3)}$. A phase field modeling approach can be used to represent the transition in diffusivities in terms of a smooth function, specifically tanh, centered about the gel-tissue interface $\phi = 0$. The appropriate function $D_i(H, \phi)$ is found to be

$$D_i(H, \phi) \quad = \quad \frac{D_i^{(3)}(H) - D_i^{(2)}(H)}{2} \tanh\left(\frac{\phi}{\epsilon}\right) + \frac{D_i^{(3)}(H) + D_i^{(2)}(H)}{2} \quad (2.13)$$

where the effect of hydrogel density on diffusivity in region (j) (where $j = 2$ is ECM and $j = 3$ is gel) is given by $D_i^{(j)}(H)$. For this model, a linear relationship

$$D_i^{(j)}(H) = D_i^{(j)}\left(1 - \frac{H}{\alpha}\right), \qquad j = 2, 3 \quad (2.14)$$

was used to capture increasing hydrogel diffusivity with degradation of the scaffold polymer.

2.2.5   Initial, Boundary, and Interface Conditions

The model is completed by specifying initial conditions on the spherical domain $(0 < r < R)$, boundary conditions at $r = 0, R$, and interface conditions along the fixed interface $r = a$. At the start of the experiment, the chondrocyte has homeostatic nutrient concentration, N_*, and there is no unlinked matrix in the system. The cell is seeded within a nutrient rich (i.e. $N = N_H \gg N_*$) hydrogel of known density H_0. The resulting initial conditions are

$$N(r, 0) \quad = \quad \begin{cases} N_*, & 0 < r < a \\ N_H, & a < r < R \end{cases}, \quad (2.15)$$

$$M(r, 0) \quad = \quad 0, \quad 0 < r < R, \quad (2.16)$$

$$H(r, 0) \quad = \quad \begin{cases} 0, & 0 < r < a \\ H_0, & a < r < R \end{cases}. \quad (2.17)$$

The level set function, ϕ, is initialized as the signed distance function $\phi = \pm d$, where d is the radial distance from the gel-tissue interface. Continuity is enforced along the

cell boundary, $r = a$, for the concentrations

$$[[N]]_{r=a} = 0, \qquad t > 0 \tag{2.18}$$

$$[[M]]_{r=a} = 0, \qquad t > 0, \tag{2.19}$$

and for the fluxes

$$D_N^{(2)} \frac{\partial N}{\partial r}\bigg|_{r=a^+} = D_N^{(1)} \frac{\partial N}{\partial r}\bigg|_{r=a^-}, \qquad t > 0 \tag{2.20}$$

$$D_M^{(2)} \frac{\partial M}{\partial r}\bigg|_{r=a^+} = D_M^{(1)} \frac{\partial M}{\partial r}\bigg|_{r=a^-}, \qquad t > 0. \tag{2.21}$$

Zero flux conditions are enforced at the center of the cell for N and M,

$$\frac{\partial N}{\partial r}\bigg|_{r=0} = 0, \qquad t > 0 \tag{2.22}$$

$$\frac{\partial M}{\partial r}\bigg|_{r=0} = 0, \qquad t > 0. \tag{2.23}$$

It is also assumed that the far-field nutrient concentration is N_H, and the unlinked matrix concentration is zero, resulting in the boundary conditions

$$N(R, t) = N_H, \qquad t > 0 \tag{2.24}$$

$$M(R, t) = 0, \qquad t > 0. \tag{2.25}$$

The cartilage regeneration model then consists of the governing equations (2.3), (2.4), (2.8)-(2.10), and (2.12) subject to the conditions in (2.15)-(2.25).

2.3 Nondimensionalization

To facilitate a parametric analysis of interactions among mechanisms captured in the model, the system is nondimensionalized using the transformations

$$\bar{N} = \frac{N}{N_*}, \qquad \bar{M} = \frac{M}{M_*}, \qquad \bar{H} = \frac{H}{H_*}, \qquad \bar{E}_H = \frac{E_H}{E_{ECM}}, \tag{2.26}$$

$$\bar{t} = \frac{t D_M^{(2)}}{a^2}, \qquad \bar{r} = \frac{r}{a}, \qquad \bar{\phi} = \frac{\phi}{a}, \qquad \bar{V}_{ECM} = \frac{V_{ECM}}{V_H(0)}, \tag{2.27}$$

where M_* and H_* are interpreted as characteristic values of M and H, respectively, that are chosen judiciously. Time, t, is scaled in terms of the slowest diffusivity $D_M^{(2)}$ in order to capture interactions on the slower scale of linked matrix accumulation that is associated with cartilage regeneration in chondrocyte-biomaterial systems. In the nondimensional system, diffusivities $D_N^{(i)}$ and $D_M^{(i)}$ are expressed by

$$\delta_N^{(i)} = \frac{D_N^{(i)}}{D_M^{(2)}}, \qquad\qquad \delta_M^{(i)} = \frac{D_M^{(i)}}{D_M^{(2)}}, \qquad\qquad i = 1, 2, 3. \qquad (2.28)$$

The reaction rates k_N, k_M, and k are now replaced with

$$\kappa_N = \frac{k_N a^2}{D_M^{(2)}}, \qquad \kappa_M = \frac{k_M E_{ECM} N_* a^2}{D_M^{(2)} M_*}, \qquad \kappa = \frac{k E_{ECM} M_* H_* a}{D_M^{(2)}}, \qquad (2.29)$$

the unlinked matrix-hydrogel reaction rates c_M and c_H become

$$\gamma_M = \frac{c_M H_* a^2}{D_M^{(2)}}, \qquad\qquad \gamma_H = \frac{c_H M_* a^2}{D_M^{(2)}}, \qquad\qquad (2.30)$$

and the hydrogel degradation rate m_H becomes

$$\mu_H = \frac{m_H a^2}{D_M^{(2)}}. \qquad\qquad (2.31)$$

The initial nutrient concentration, N_H, initial hydrogel density, H_0, and the initial hydrogel stiffness, E_{H_0}, are now represented by

$$\bar{N}_H = \frac{N_H}{N_*}, \qquad\qquad \bar{H}_0 = \frac{H_0}{H_*}, \qquad\qquad \bar{E}_{H_0} = \frac{E_{H_0}}{E_{ECM}}, \qquad (2.32)$$

and the domain boundary R becomes $\bar{R} = \frac{R}{a}$.

Substituting (2.26) and (2.27) into (2.3) and (2.4) yields the nondimensional model

$$\frac{\partial \bar{N}}{\partial \bar{t}} = \delta_N^{(1)} \nabla^2 \bar{N} - \kappa_N \left(\bar{N} - 1\right), \qquad\qquad 0 < \bar{r} < 1,\ \bar{t} > 0,$$

$$(2.33)$$

$$\frac{\partial \bar{M}}{\partial \bar{t}} = \delta_M^{(1)} \nabla^2 \bar{M} + \kappa_M \left(1 - \bar{E}_H(\bar{t})\right) \left(1 - \bar{V}_{ECM}(\bar{t})\right) \left(\bar{N} - 1\right), \quad 0 < \bar{r} < 1,\ \bar{t} > 0.$$

$$(2.34)$$

Similarly, transformation of (2.8)-(2.10) gives

$$\frac{\partial \bar{N}}{\partial \bar{t}} = \nabla \cdot \left(\delta_N^{(2,3)} \left(\bar{H}, \bar{\phi} \right) \nabla \bar{N} \right), \qquad\qquad 1 < \bar{r} < \bar{R}, \ \bar{t} > 0, \qquad (2.35)$$

$$\frac{\partial \bar{M}}{\partial \bar{t}} = \nabla \cdot \left(\delta_M^{(2,3)} \left(\bar{H}, \bar{\phi} \right) \nabla \bar{M} \right) - \gamma_M \bar{M} \bar{H}, \qquad 1 < \bar{r} < \bar{R}, \ \bar{t} > 0, \qquad (2.36)$$

$$\frac{\partial \bar{H}}{\partial \bar{t}} = -\gamma_H \bar{M} \bar{H} - \mu_H \bar{H}, \qquad\qquad 1 < \bar{r} < \bar{R}, \ \bar{t} > 0. \qquad (2.37)$$

Substituting the scaled variables into (2.12) results in the nondimensional level set equation

$$\frac{d\bar{\phi}}{d\bar{t}} + \bar{F} \left| \nabla \bar{\phi} \right| = 0, \quad \bar{F} = \kappa \left(1 - \bar{E}_H(\bar{t}) \right) \left(1 - \bar{V}_{ECM}(\bar{t}) \right) \bar{M} \bar{H}, \quad 1 < \bar{r} < \bar{R}, \ \bar{t} > 0$$

$$(2.38)$$

To complete the nondimensionalized model, the initial conditions (2.15)-(2.17) transform to

$$\bar{N}(\bar{r}, 0) = \begin{cases} 1, & 0 < \bar{r} < 1 \\ \bar{N}_H, & 1 < \bar{r} < \bar{R} \end{cases} \qquad (2.39)$$

$$\bar{M}(\bar{r}, 0) = 0, \quad 0 < \bar{r} < \bar{R} \qquad (2.40)$$

$$\bar{H}(\bar{r}, 0) = \begin{cases} 0, & 0 < \bar{r} < 1 \\ \bar{H}_0, & 1 < \bar{r} < \bar{R}. \end{cases} \qquad (2.41)$$

Similarly, the interface continuity conditions (2.18)-(2.21) become

$$\left[\left[\bar{N}\right]\right]_{\bar{r}=1} = 0, \qquad\qquad \left[\left[\bar{M}\right]\right]_{\bar{r}=1} = 0, \qquad\qquad \bar{t} > 0, \qquad (2.42)$$

and

$$\delta_N^{(2)} \frac{\partial \bar{N}}{\partial \bar{r}} \bigg|_{\bar{r}=1^+} = \delta_N^{(1)} \frac{\partial \bar{N}}{\partial \bar{r}} \bigg|_{\bar{r}=1^-}, \qquad \delta_M^{(2)} \frac{\partial \bar{M}}{\partial \bar{r}} \bigg|_{\bar{r}=1^+} = \delta_M^{(1)} \frac{\partial \bar{M}}{\partial \bar{r}} \bigg|_{\bar{r}=1^-}, \qquad \bar{t} > 0. \qquad (2.43)$$

Lastly, the zero flux conditions (2.22)-(2.23) become

$$\frac{\partial \bar{N}}{\partial \bar{r}} \bigg|_{\bar{r}=0} = 0, \qquad\qquad \frac{\partial \bar{M}}{\partial \bar{r}} \bigg|_{\bar{r}=0} = 0, \qquad\qquad \bar{t} > 0, \qquad (2.44)$$

and the boundary conditions (2.24)-(2.25) are transformed into

$$\bar{N}(\bar{R}, \bar{t}) = \bar{N}_H, \qquad\qquad \bar{M}(\bar{R}, \bar{t}) = 0, \qquad\qquad \bar{t} > 0. \qquad (2.45)$$

The nondimensional model (2.33)-(2.38) subject to the conditions (2.39)-(2.45) will be used throughout the rest of this chapter.

2.4 Numerical Methods

2.4.1 Finite Difference Method

In order to numerically approximate solutions to the reaction-diffusion equations, (2.33) and (2.34) are discretized using implicit backward Euler schemes that are first-order in time and second-order in space. Let $N_i^j = N(r_i, t_j)$ and $M_i^j = M(r_i, t_j)$ for $i = 1, 2, \ldots, I_C - 1$, $j = 1, 2, \ldots, J_T$, where $r_i = i\Delta\bar{r}$, $I_C = \frac{1}{\Delta\bar{r}}$, and J_T is the total number of time steps. The index I_C corresponds to the node located at the cell boundary $r = a$. In our numerical scheme, the time step $\Delta\bar{t}$ will vary to allow for efficient computations on the slow time scales associated with cartilage regeneration. Details for choosing the values of $\Delta\bar{t}$ and $\Delta\bar{r}$ can be found in Section 2.4.3. The resulting finite difference scheme for N_i^j and M_i^j in (2.33) and (2.34) are, respectively,

$$\left(\frac{\delta_N^{(1)}}{(\Delta r)^2} - \frac{\delta_N^{(1)}}{2r_i \Delta r}\right) N_{i-1}^{j+1} + \left(\frac{-2\delta_N^{(1)}}{(\Delta r)^2} - \frac{1}{\Delta t} - \kappa_N\right) N_i^{j+1} + \left(\frac{\delta_N^{(1)}}{(\Delta r)^2} + \frac{\delta_N^{(1)}}{2r_i \Delta r}\right) N_{i+1}^{j+1}$$

$$= \frac{-N_i^j}{\Delta t} - \kappa_N, \quad (2.46)$$

$$\left(\frac{\delta_M^{(1)}}{(\Delta r)^2} - \frac{\delta_M^{(1)}}{2r_i \Delta r}\right) M_{i-1}^{j+1} + \left(\frac{-2\delta_M^{(1)}}{(\Delta r)^2} - \frac{1}{\Delta t}\right) M_i^{j+1} + \left(\frac{\delta_M^{(1)}}{(\Delta r)^2} + \frac{\delta_M^{(1)}}{2r_i \Delta r}\right) M_{i+1}^{j+1}$$

$$= \frac{-M_i^j}{\Delta t} - \kappa_M \left(1 - E_H^j\right) \left(1 - V_{ECM}^j\right) \left(N_i^{j+1} - 1\right). \quad (2.47)$$

Equations (2.35) and (2.36) are discretized in the same way, resulting in the following scheme for points outside of the cell, $i = I_C, I_C + 1, \ldots, I_R$ ($I_R = \frac{\bar{R}}{\Delta \bar{r}}$) and $j = 1, 2, \ldots, J_T$,

$$
\left(\frac{\alpha_i^j}{(\Delta r)^2} - \frac{\alpha_i^j}{r_i \Delta r} - \frac{\alpha_{i,r}^j}{2\Delta r} \right) N_{i-1}^{j+1} + \left(-\frac{2\alpha_i^j}{(\Delta r)^2} - \frac{1}{\Delta t} \right) N_i^{j+1}
$$
$$
+ \left(\frac{\alpha_i^j}{(\Delta r)^2} + \frac{\alpha_i^j}{r_i \Delta r} + \frac{\alpha_{i,r}^j}{2\Delta r} \right) N_{i+1}^{j+1} = \frac{-N_i^j}{\Delta t}, \qquad (2.48)
$$

$$
\left(\frac{\beta_i^j}{(\Delta r)^2} - \frac{\beta_i^j}{r_i \Delta r} - \frac{\beta_{i,r}^j}{2\Delta r} \right) M_{i-1}^{j+1} + \left(-\frac{2\beta_i^j}{(\Delta r)^2} - \frac{1}{\Delta t} - \gamma_M H_I^j \right) M_i^{j+1}
$$
$$
+ \left(\frac{\beta_i^j}{(\Delta r)^2} + \frac{\beta_i^j}{r_i \Delta r} + \frac{\beta_{i,r}^j}{2\Delta r} \right) M_{i+1}^{j+1} = \frac{-M_i^j}{\Delta t}, \qquad (2.49)
$$

where $\alpha_i^j = \delta_N^{(2,3)}(r_i, t_j)$ and $\beta_i^j = \delta_M^{(2,3)}(r_i, t_j)$. The derivatives of these diffusivity expressions, denoted by $\alpha_{i,r}^j$ and $\beta_{i,r}^j$, respectively, are found by the chain rule. For α_i^j the result is

$$
\frac{\partial \delta_N^{(2,3)}}{\partial r} = \frac{\partial \delta_N^{(2,3)}}{\partial H} \frac{\partial H}{\partial r} + \frac{\partial \delta_N^{(2,3)}}{\partial \phi} \frac{\partial \phi}{\partial r}, \qquad (2.50)
$$

$$
\alpha_{i,r}^j = \left. \frac{\partial \delta_N^{(2,3)}}{\partial H} \right|_{\substack{H=H_i^j \\ \phi=\phi_i^j}} \frac{H_{i+1}^j - H_{i-1}^j}{2\Delta r} + \left. \frac{\partial \delta_N^{(2,3)}}{\partial \phi} \right|_{\substack{H=H_i^j \\ \phi=\phi_i^j}} \frac{\phi_{i+1}^j - \phi_{i-1}^j}{2\Delta r}, \qquad (2.51)
$$

where $\frac{\partial \delta_N^{(2,3)}}{\partial H}$ is determined analytically. Similar derivatives are computed for β_i^j. The continuity conditions (2.42) and (2.43) are discretized to become

$$
N_{I_C-1}^{j+1} - N_{I_C}^{j+1} = 0, \qquad\qquad M_{I_C-1}^{j+1} - M_{I_C}^{j+1} = 0, \qquad (2.52)
$$

and

$$
\delta_N^{(1)} N_{I_C-2}^{j+1} - \delta_N^{(1)} N_{I_C-1}^{j+1} - \delta_N^{(2)} N_{I_C}^{j+1} + \delta_N^{(2)} N_{I_C+1}^{j+1} = 0, \qquad (2.53)
$$
$$
\delta_M^{(1)} M_{I_C-2}^{j+1} - \delta_M^{(1)} M_{I_C-1}^{j+1} - \delta_M^{(2)} M_{I_C}^{j+1} + \delta_M^{(2)} M_{I_C+1}^{j+1} = 0. \qquad (2.54)
$$

Similarly, the zero flux conditions (2.44) become

$$
N_1^{j+1} - N_2^{j+1} = 0, \qquad\qquad M_1^{j+1} - M_2^{j+1} = 0, \qquad (2.55)
$$

and the boundary conditions (2.45) are given by

$$N_{I_R}^{j+1} = \bar{N}_H, \qquad\qquad M_{I_R}^{j+1} = 0. \tag{2.56}$$

Subsequent to assembly, the equations in (2.46)-(2.56) form two linear systems of the form

$$\mathbf{A}_N \vec{N} = \vec{b}_N, \qquad\qquad \mathbf{A}_M \vec{M} = \vec{b}_M, \tag{2.57}$$

for each time step $j = 1, 2, \ldots, J_T$. The matrices $\mathbf{A}_N$ and $\mathbf{A}_M$ are sparse, with entries only along diagonally central bands. Solutions to the linear systems (2.57) are computed using the sparse matrix solver in MATLAB.

Equations (2.37) and (2.38) are approximated using explicit first-order methods via

$$H_i^{j+1} = \left(1 - \Delta t \left(\gamma_H M_i^{j+1} + \mu_H\right)\right) H_i^j, \tag{2.58}$$

and

$$\phi_i^{j+1} = \phi_i^j - \frac{\Delta t}{\Delta r} F_i^j \left|\phi_i^j - \phi_{i-1}^j\right|, \tag{2.59}$$

$$F_i^j = \kappa \left(1 - (E_H)_i^j\right) \left(1 - (V_{ECM})_i^j\right) M_i^j H_i^j, \tag{2.60}$$

where i, j are defined as before.

2.4.2 Initialization

The initial conditions (2.39)-(2.41) correspond to values for N, M, and H at time $t = 0$ (i.e. the initial time step $j = 1$) that are set to be

$$N_i^1 = \begin{cases} 1, & i = 1, 2, \ldots, I_C - 1 \\ \bar{N}_H, & i = I_C, I_C + 1, \ldots, I_R \end{cases}, \tag{2.61}$$

$$M_i^1 = 0, \quad i = 1, 2, \ldots, I_R, \tag{2.62}$$

$$H_i^1 = \begin{cases} 0, & i = 1, 2, \ldots, I_C - 1 \\ \bar{H}_0, & i = I_C, I_C + 1, \ldots, I_R \end{cases}. \tag{2.63}$$

Note that at $t = 0$, there is no linked ECM region and, hence, no natural spatial location for the interface corresponding to the level set $\phi = 0$. To prevent numerical issues that could result from the creation of this region during early time steps, the $j = 2$ step is taken with the assumption that the interface ($\phi = 0$) has advanced by an amount equal to 2% of the cell radius, or 4 grid points. This automatically creates an ECM region with a volume of less than 0.05% of the target ECM volume that is determined by the geometric parameter $\bar{R}$. Because the initial step is so small, any resulting inaccuracy in the linked matrix regeneration time will be roughly less than a day (in true dimensional variables) and, thus, considered negligible on the longer time scales of several weeks to a few months associated with cartilage regeneration and scaffold degradation. Once N, M, H, and ϕ have been updated for $j = 2$, all later iterations ($j = 3, 4, \ldots, J_T$) are performed as described in Section 2.4.1 above.

2.4.3 Stability and Convergence

The Courant-Friedrichs-Lewy condition (or CFL condition) is used to enforce stability in level set methods [26]. The time step, $\Delta \bar{t}$, is restricted by the expression

$$\Delta \bar{t} \left(\frac{\max \left\{ |\bar{F}| \right\}}{\Delta \bar{r}} \right) = \alpha \tag{2.64}$$

where α is known as a CFL number, and is chosen such that $0 < \alpha < 1$, where $\max \left\{ |\bar{F}| \right\}$ is the maximum value of $|\bar{F}|$, from (2.38), over the entire domain. While this condition helps to restrict the time step, it is also important that a sufficiently small spatial step, $\Delta \bar{r}$, be used. A mesh refinement study was performed, and $\Delta \bar{r} = 0.005$ was chosen in order to balance accuracy and efficiency in the model simulations (see Figure 2.4).
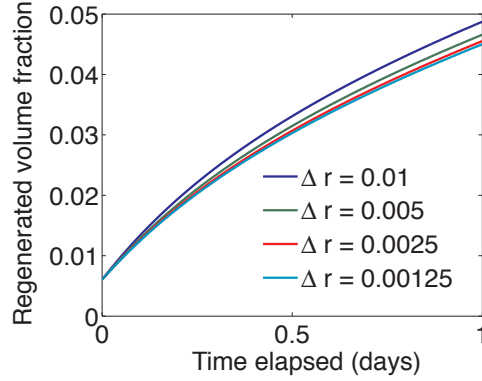
Figure 2.4: A mesh refinement study was performed in order to establish an appropriate step size $\Delta \bar{r}$ that would balance accuracy and efficiency of the numerical methods.

2.5   Reduced Model: Constant Nutrients

Because the hydrogel is nutrient-rich and nutrient solute size is much less than that of unlinked matrix, nutrient diffusion is typically an order of magnitude faster than unlinked matrix diffusion. This motivates the examination of a reduced model in which the equations (2.33) and (2.35) and the corresponding initial, interface, and boundary conditions are replaced by the uniform nutrient concentration assumption

$$\bar{N}\left(\bar{r}, \bar{t}\right) \equiv \bar{N}_H, \qquad\qquad 0 \leq \bar{r} \leq \bar{R}, \ \bar{t} \geq 0. \qquad (2.65)$$

This simplification eliminates the need to solve the spare matrix system $\mathbf{A}_N \vec{N} = \vec{b}_N$ and can reduce computing time without significantly affecting model accuracy

Chapter 3

Reaction-Diffusion Model: Parametric Analysis and Results

3.1 Introduction

In this chapter, results are presented for the models described in Chapter 2. The different types of parameters will be summarized, and the choice of values or ranges for each parameter will be explained. A parametric analysis was also performed, focusing on the dependence of ECM regeneration times on model parameters. In several cases, these relationships can be described via power laws. Possible model reductions are also briefly explored. One of the overall objectives of analyzing regeneration times is to use the spatially-meaningful parameters to quantitatively categorize hydrogels in order to streamline future cartilage regeneration experiments for accelerated realization of optimal functional outcomes. Within this context, regeneration times for systems with chondrocytes seeded into biomaterial scaffolds range from a few weeks to several months. The analysis was calibrated to maintain values in these intervals.

3.2   Selection of Model Parameters

Parameters contained in the model described in Chapter 2 can be separated into three primary categories: biophysical parameters, scaffold design parameters, and physiological parameters. There is also a fourth group of geometric parameters, which are less meaningful from a tissue engineering standpoint, but necessary for computing a solution. Since $a = 5$ μm is a typical radius of a chondrocyte [10], and $R \gg a$, the cell-tissue interface in the non-dimensional model is located at $\bar{r} = 1$ and the outer hydrogel boundary is located at $\bar{R} = 5$. The parameters ϵ and α in the phase field model of diffusivity (2.13)-(2.14) are taken to be $\epsilon = 0.1$ and $\alpha = 5$.

3.2.1   Biophysical Parameters

The diffusivities fall under the category of biophysical parameters, and can be chosen based on previous experimental studies. Leddy et al. [15, 16] have conducted studies of molecular diffusion with varying solute size in several scaffolds and in articular cartilage ECM via photobleaching techniques. As defined in (2.28), the diffusivities in our model are normalized relative to the diffusivity of free matrix in the ECM region, i.e.

$$\delta_M^{(2)} = 1. \tag{3.1}$$

The reference diffusivity used to nondimensionalize the others is taken to be $D_M^{(2)} = 6$ μm^{2}s^{-1}, which is the literature value of the diffusion coefficient for a 500 kDa molecule in native cartilage [15]. Since diffusivity increases as particle size decreases, and nutrients are much smaller than matrix molecules, we assume that

$$\delta_M^{(i)} < \delta_N^{(i)} \text{ for } i = 1, 2, 3, \tag{3.2}$$

where it is recalled that $i = 1$ denotes the intracellular region, $i = 2$ denotes the ECM region, and $i = 3$ denotes the hydrogel region. Based on the literature [15],

$$\delta_N^{(2)} = 15 \tag{3.3}$$

is determined to be a reasonable value for the diffusivity of nutrients in articular cartilage ECM. Diffusivity in the hydrogel is dependent upon the characteristics of the specific scaffold material, and we consider the range of possible parameter values as $60 < \delta_N^{(3)} < 360$ and $2 < \delta_M^{(3)} < 50$. The $\delta_N^{(3)}$ range was determined from experimental values for small dextrans in different scaffolds, and the $\delta_M^{(3)}$ range was determined from the measurements for larger dextrans [15]. The value

$$\delta_M^{(3)} = 20 \tag{3.4}$$

was chosen as the baseline value in this study, and based on (3.2), we chose

$$\delta_N^{(3)} = 10\delta_M^{(3)} = 200. \tag{3.5}$$

At present, data is unavailable for solute diffusivity within a chondrocyte. For the purposes of this study it is assumed that nutrient and free matrix diffusivities lie between those for the hydrogel and the cartilage ECM so that

$$\delta_j^{(2)} < \delta_j^{(1)} < \delta_j^{(3)} \text{ for } j = N, M. \tag{3.6}$$

This choice is motivated by the dense structure of the ECM relative to the cell, as well as the observation that the inhomogeneous and complex intracellular environment could inhibit diffusion as compared to the more homogenous environment of the scaffold. As a result, the values chosen in this study are

$$\delta_M^{(1)} = 10, \tag{3.7}$$

$$\delta_N^{(1)} = 10\delta_M^{(1)} = 100. \tag{3.8}$$

The choice for baseline values of all of the biophysical parameters, i.e. (3.1),(3.3)-(3.5), and (3.7)-(3.8), are summarized in Table 3.1.

3.2.2 Scaffold Design Parameters

The scaffold design parameters include the initial scaffold nutrient concentration, $\bar{N}_H$, as well as the initial density and stiffness of the hydrogel ($\bar{H}_0$ and $\bar{E}_{H_0}$, respectively). These are measurable values that are dependent on the particular hydrogel

being investigated, and are controlled by the experimentalist. Since hydrogels are typically nutrient-rich, it is assumed that $\bar{N}_H$ is one order of magnitude greater than the homeostatic nutrient level, $\bar{N}_* = 1$, so that

$$\bar{N}_H \;\; = \;\; 10. \tag{3.9}$$

It is also assumed that

$$\bar{H}_0 \;\; = \;\; 2.5, \tag{3.10}$$

$$\bar{E}_{H_0} \;\; = \;\; 0.001. \tag{3.11}$$

The initial stiffness is estimated from literature values for ECM and hydrogel Young's modulus [22]. The scaffold design parameter values are summarized in Table 3.2.

3.2.3   Physiological Parameters

Lastly, the physiological parameters represent the underlying cell biological mechanisms in the model which include the rates of nutrient utilization, matrix synthesis, ECM linking, matrix and hydrogel reactions, and hydrogel degradation. These parameters are difficult to determine experimentally, but ultimately could be obtained via parameter estimation in which models of cartilage regeneration are fit to experimental data. Indeed, these parameters may often be the quantities of interest in quantifying and comparing different cell-biomaterial systems in tissue engineering applications. For the current study, it is assumed that all of these processes occur on a slower scale than diffusion, and referring to (2.33)-(2.38), that the approximate ordering of these parameters is

$$\mu_H < \gamma_H < \gamma_M \leq \kappa < \kappa_M < \kappa_N < 1. \tag{3.12}$$

The nutrient utilization rate, κ_N is assumed to be the fastest of all of these rates and is chosen to be

$$\kappa_N \;\; = \;\; 0.1. \tag{3.13}$$

The next fastest rate is assumed to be the rate of unlinked matrix synthesis,

$$\kappa_M = 0.01, \tag{3.14}$$

followed by the hydrogel-ECM linking rate

$$\kappa = 0.001. \tag{3.15}$$

It is assumed that the unlinked matrix reaction rate, γ_M, which describes the rate at which unlinked matrix is taken out of the system as a result of linking guided by the scaffold, is on the same order as the linking rate (3.15). Therefore,

$$\gamma_M = 0.001 \tag{3.16}$$

is selected. The hydrogel reaction rate, which describes the rate at which hydrogel is taken out of the system as a result of linking, is assumed to be much slower, and the inherent hydrogel degradation is assumed to occur on an even slower scale, so that

$$\gamma_H = 0.00005, \tag{3.17}$$

$$\mu_H = 0.000001. \tag{3.18}$$

Overall, the ECM accumulation and structural integrity of the regenerated tissue is strongly influenced by the rate of hydrogel degradation. If the scaffold degrades too quickly, defects could appear; if it degrades too slowly, it could inhibit ECM accumulation by preventing timely diffusive transport of the ECM molecules [29]. Due to the absence of detailed spatial and temporal data for estimation of the physiological parameters in (3.13)-(3.18), the choices made above were also influenced by calibration of linked matrix regeneration times to realistic ranges for engineered cartilage. The physiological parameters are summarized in Table 3.3.

Table 3.1: A table of baseline biophysical parameter values for analysis of the reaction-diffusion model.

Parameter	Definition	Description	Value
$\delta_N^{(1)}$	$D_N^{(1)}/D_M^{(2)}$	N diffusion in cell	100
$\delta_N^{(2)}$	$D_N^{(2)}/D_M^{(2)}$	N diffusion in ECM	15
$\delta_N^{(3)}$	$D_N^{(3)}/D_M^{(2)}$	N diffusion in hydrogel	200
$\delta_M^{(1)}$	$D_M^{(1)}/D_M^{(2)}$	M diffusion in cell	10
$\delta_M^{(2)}$	$D_M^{(2)}/D_M^{(2)}$	M diffusion in ECM	1
$\delta_M^{(3)}$	$D_M^{(3)}/D_M^{(2)}$	M diffusion in hydrogel	20

Table 3.2: A table of the baseline scaffold design parameter values for analysis of the reaction-diffusion model.

Parameter	Definition	Description	Value
$\bar{N}_H$	N_H/N_*	Initial hydrogel nutrients	10
$\bar{H}_0$	H_0/H_*	Initial hydrogel density	2.5
$\bar{E}_{H_0}$	E_{H_0}/E_{ECM}	Initial hydrogel stiffness	0.001

Table 3.3: A table of baseline physiological parameter values for analysis of the reaction-diffusion model.

Parameter	Definition	Description	Value
κ_N	$k_N a^2/D_M^{(2)}$	Nutrient absorption rate	0.1
κ_M	$k_M E_{ECM} N_* a^2/D_M^{(2)} M_*$	Unlinked matrix synthesis rate	0.01
κ	$k E_{ECM} M_* H_* a/D_M^{(2)}$	Hydrogel-ECM linking rate	0.001
γ_M	$c_M H_* a^2/D_M^{(2)}$	Unlinked matrix reaction rate	0.001
γ_H	$c_H M_* a^2/D_M^{(2)}$	Hydrogel reaction rate	0.00005
μ_H	$m_H a^2/D_M^{(2)}$	Hydrogel degradation rate	0.000001

3.3   Baseline Case

The baseline case for the model (2.33)-(2.38) subject to the conditions (2.39)-(2.45) is defined by the parameter values summarized in Tables 3.1, 3.2, and 3.3. Numerical solutions were computed using the techniques described in Section 2.4. Two different representations for simulated spatial profiles of unlinked matrix concentration at multiple points in time are shown in Figures 3.1 and 3.2. Similar profiles for nutrient concentration are shown in Figures 3.3 and 3.4.

Recalling that $\bar{r} = 1$ is the location of the cell boundary, it is first observed that nutrient profiles remain almost unchanged. This is due to the fast diffusivities of small solutes in all three regions, as well as the boundary condition in (2.45) which sustains nutrient availability at the prescribed level $\bar{N}_H = 10$. Matrix profiles exhibit significant spatial and temporal variations due to the slower rates associated with the associated mechanisms. The model simulations exhibit steeper gradients in the extracellular region due to the complex interactions between synthesized matrix and the hydrogel.
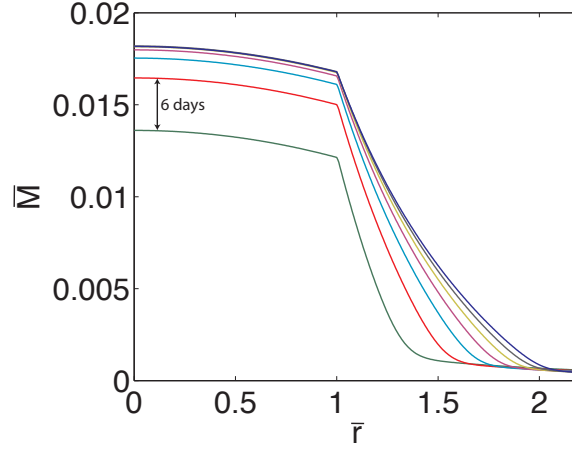
Figure 3.1: Spatial profiles of unlinked matrix concentration, $\bar{M}$, for the baseline case. Note that the cell boundary is located at $\bar{r} = 1$, and successive curves advance upwards at intervals of 6 days.
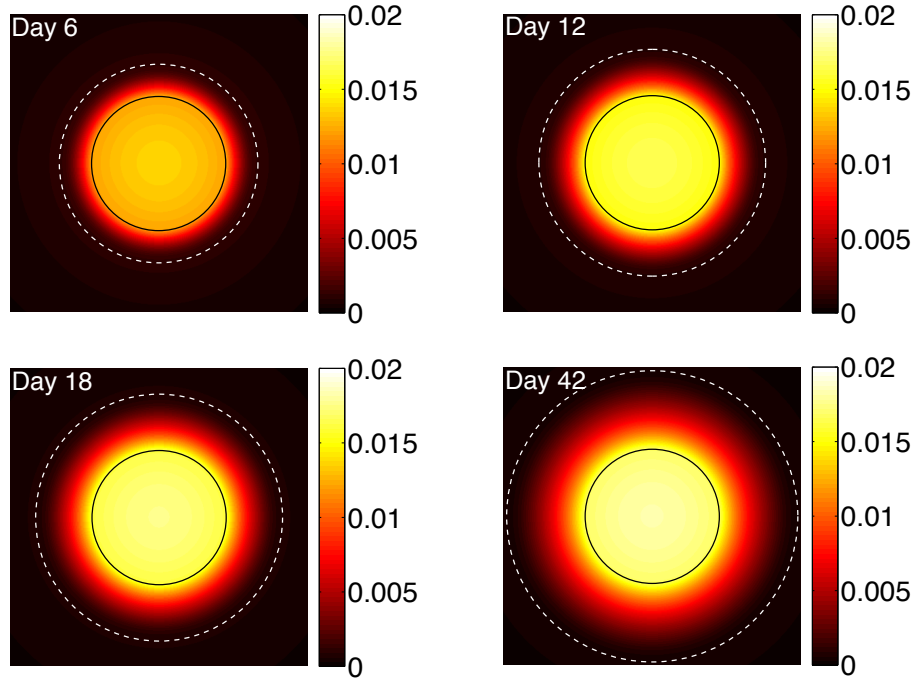
Figure 3.2: Spatial maps of unlinked matrix concentration, $\bar{M}$, for the baseline case. The black solid line represents the cell boundary, and the white dashed line represents the location of the $\bar{\phi} = 0$ interface separating the linked ECM and hydrogel regions.
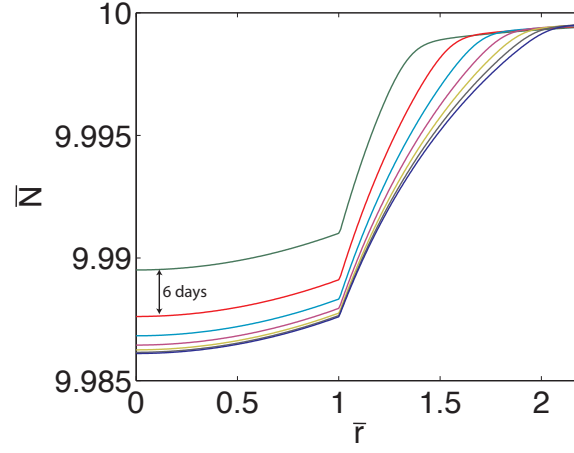
Figure 3.3: Spatial profiles of nutrient concentration, $\bar{N}$, for the baseline case. Note that the cell boundary is located at $\bar{r} = 1$, and successive curves advance downwards at intervals of 6 days.
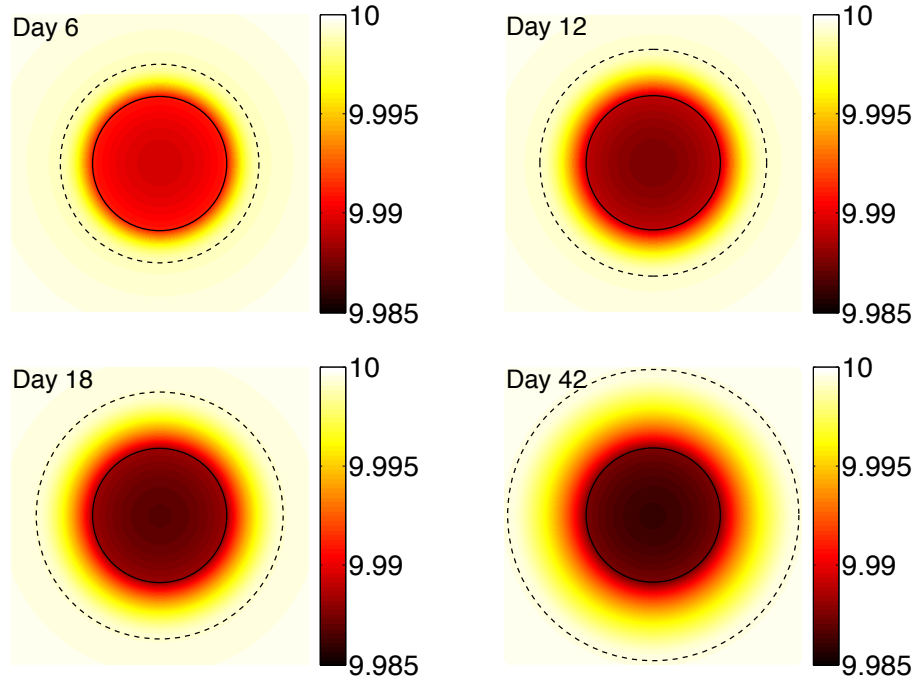
Figure 3.4: Spatial maps of nutrient concentration, $\bar{N}$, for the baseline case. The black solid line represents the cell boundary, and the white dashed line represents the location of the $\bar{\phi} = 0$ interface separating the linked ECM and hydrogel regions.

3.4 Parametric Analysis of Cartilage Regeneration

For the purposes of this study, it is assumed that the target regenerated tissue volume is 10 times the volume of the chondrocyte, or $V_{target} = 10V_{cell}$. In nondimensional coordinates, $V_{cell} = \frac{4}{3}\pi$, and thus the regenerated ECM volume fraction is

$$\tilde{V}_{ECM}(\bar{t}) = \frac{\bar{r}_{ECM}^3 - 1}{10}, \text{ where } \phi\left(\bar{r}_{ECM}, \bar{t}\right) = 0. \tag{3.19}$$

Note that $\bar{r}_{ECM}$ is the location of the hydrogel-ECM interfacial region at time $\bar{t}$. The regeneration time, T_{regen} is computed as the time at which the regenerated ECM volume fraction first exceeds 95 %, or

$$\min\left\{T_{regen} : \bar{V}_{ECM}(T_{regen}) \geq 0.95\right\}. \tag{3.20}$$

3.4.1 Biophysical Parameters

Based on Section 3.2, the rate of unlinked matrix diffusion through the hydrogel, denoted by $\delta_M^{(3)}$, was varied in the interval $2 < \delta_M^{(3)} < 50$, and on a slower time scale than nutrient diffusion. Three values, $\delta_M^{(3)} = 15$, $\delta_M^{(3)} = 20$, $\delta_M^{(3)} = 25$ were considered in order to keep regeneration times in a realistic range. Regeneration curves are shown in Figure 3.5(a). For $\delta_M^{(3)} = 15$ the regeneration time was computed to be $T_{regen} = 28.5$ days, for $\delta_M^{(3)} = 20$ it was $T_{regen} = 44.1$ days, and for $\delta_M^{(3)} = 25$ it was $T_{regen} = 67.2$ days. Increasing $\delta_M^{(3)}$ slowed down the tissue regeneration process, increasing T_{regen}. This might seem counterintuitive at first, but can be explained by the unlinked matrix diffusing through the linked matrix interface and into the hydrogel region. As a result, the formation of linked ECM near $\bar{\phi} = 0$ occurs less efficiently. Spatial profiles of the unlinked matrix concentration for these three cases are shown in Figures 3.5(b)-(d). In the region near $\bar{r} = 1$ these profiles illustrate how accumulation of unlinked matrix near the cell interface slows down with increasing diffusivity of unlinked matrix.

3.4.2 Scaffold Design Parameters

Since hydrogels tend to be nutrient-rich, the initial nutrient concentration of the hydrogel, $\bar{N}_H$, is assumed to be much larger than the homeostatic nutrient level, i.e. $\bar{N}_H \gg 1$. The values chosen for this study were $\bar{N}_H = 10$, $\bar{N}_H = 15$, and $\bar{N}_H = 20$. Regeneration curves are shown in Figure 3.6(a). For $\bar{N}_H = 10$ the regeneration time was $T_{regen} = 44.1$ days, for $\bar{N}_H = 15$ it was $T_{regen} = 22.5$ days, and for $\bar{N}_H = 20$ it was $T_{regen} = 15.2$ days. We observe that increasing $\bar{N}_H$ has exactly the effect one might expect; excess nutrients allow unlinked matrix to be synthesized more quickly, which results in more rapid linking of ECM. Spatial profiles of the unlinked matrix concentration for these three cases support this observation, as illustrated in Figures 3.6(b)-(d), and reflected by increasing intracellular concentration of $\bar{M}$ as $\bar{N}_H$ is increased.

Variations of the initial hydrogel stiffness, $\bar{E}_{H_0}$, had significantly less impact on regeneration time when changed by two orders of magnitude. In particular, for $\bar{E}_{H_0} = 0.0001$, $T_{regen} = 44$ days, for $\bar{E}_{H_0} = 0.001$, $T_{regen} = 44.1$ days, and for $\bar{E}_{H_0} = 0.01$, $T_{regen} = 45.6$ days. Increasing the parameter further, to a value of $\bar{E}_{H_0} = 0.1$ did result in a large increase in regeneration time ($T_{regen} = 66.5$ days), but this large value falls outside the reasonable range of hydrogel stiffness.

Perturbations to the initial hydrogel density, $\bar{H}_0$, were also studied. Regeneration curves are shown in Figure 3.7(a) for the cases $\bar{H}_0 = 2$, $\bar{H}_0 = 2.5$, and $\bar{H}_0 = 3$. The corresponding regeneration times were $T_{regen} = 83.4$ days, $T_{regen} = 44.1$ days, and $T_{regen} = 26.3$ days, respectively. It is observed that increasing $\bar{H}_0$ while leaving the other parameters fixed results in a decreased T_{regen}, suggesting that the gel-matrix reaction occurs faster for an initially denser hydrogel scaffold.

3.4.3 Physiological Parameters

The hydrogel-ECM linking rate, κ, in (2.38) controls a mechanism that occurs on a much slower time scale than diffusion, nutrient absorption, and unlinked matrix synthesis. Therefore the three values chosen were $\kappa = 0.001$, $\kappa = 0.002$, and

$\kappa = 0.003$, and the associated regeneration curves are shown in Figure 3.8(a). The corresponding regeneration times were found to be $T_{regen} = 44.1$ days for $\kappa = 0.001$, $T_{regen} = 16.3$ days for $\kappa = 0.002$, and $T_{regen} = 10.0$ days for $\kappa = 0.003$, reflecting a high sensitivity in which regeneration time decreases significantly with increasing κ. Spatial profiles of the unlinked matrix concentration for these three cases are shown in Figures 3.8(b)-(d).

The unlinked matrix synthesis rate, κ_M, was examined in the cases $\kappa_M = 0.01$, $\kappa_M = 0.015$, and $\kappa_M = 0.02$. Corresponding regeneration curves are shown in Figure 3.9(a). The regeneration times were found to be $T_{regen} = 44.1$ days for $\kappa_M = 0.01$, $T_{regen} = 23.7$ days for $\kappa_M = 0.015$, and $T_{regen} = 16.2$ days for $\kappa_M = 0.02$. Note that doubling the baseline value results in almost exactly the same change in regeneration time as the same action in κ, above. Since increasing κ_M results in a faster production of unlinked matrix available for linking, increasing this parameter decreases regeneration time. Spatial profiles of the unlinked matrix concentration for these three cases are found in Figures 3.9(b)-(d).

The other four physiological parameters were not examined for this parametric analysis. The nutrient absorption rate, κ_N, is on such a fast scale that its effect is essentially negligible. This assumption is further supported by the results in Section 3.5. The unlinked matrix and hydrogel reaction rates, γ_M and γ_H, as well as the hydrogel degradation rate, μ_H, were not studied because they are much slower underlying mechanisms that are not directly responsible for the creation of new matrix (linked or unlinked), as in (3.12).
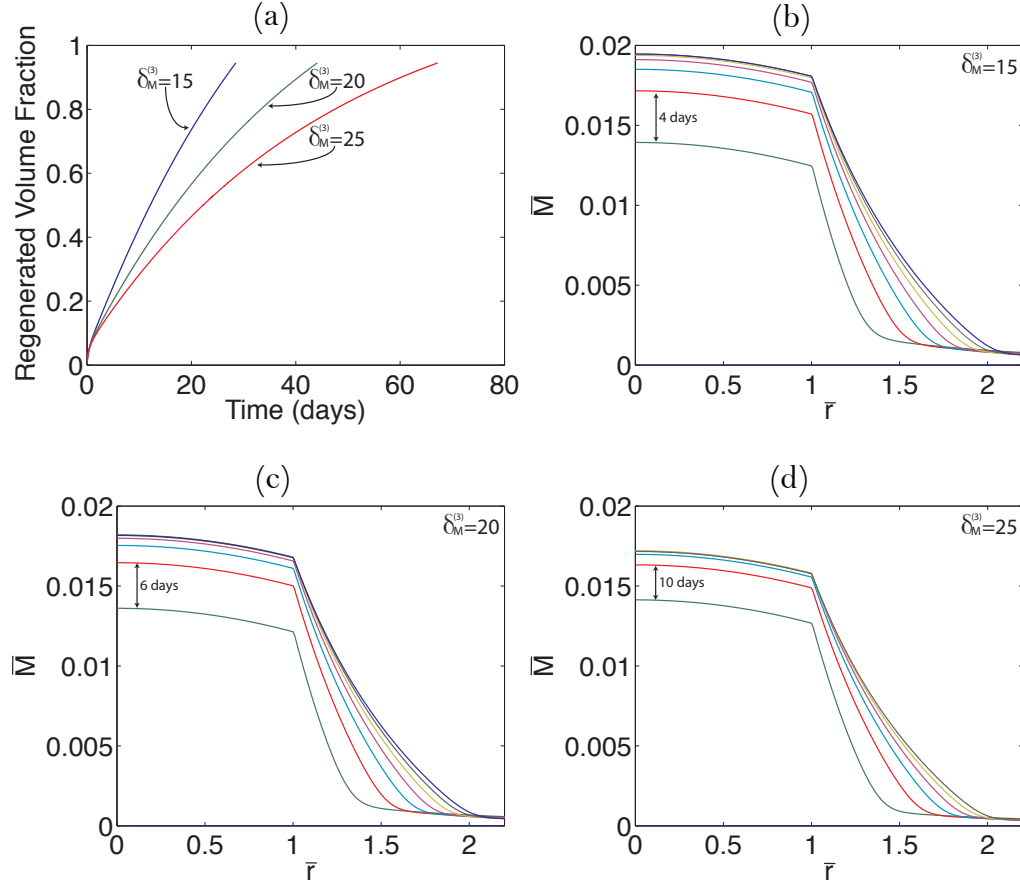
Figure 3.5: (a) A plot of regenerated volume fraction $\tilde{V}_{ECM}(\bar{t})$ for three values of $\delta_M^{(3)}$. (b) The case $\delta_M^{(3)} = 15$, for which $T_{regen} = 28.5$ days. Successive curves advance upwards at intervals of 4 days. (c) The case $\delta_M^{(3)} = 20$, for which $T_{regen} = 44.1$ days. Successive curves advance upwards at intervals of 6 days. (d) The case $\delta_M^{(3)} = 25$, for which $T_{regen} = 67.2$ days. Successive curves advance upwards at intervals of 10 days.
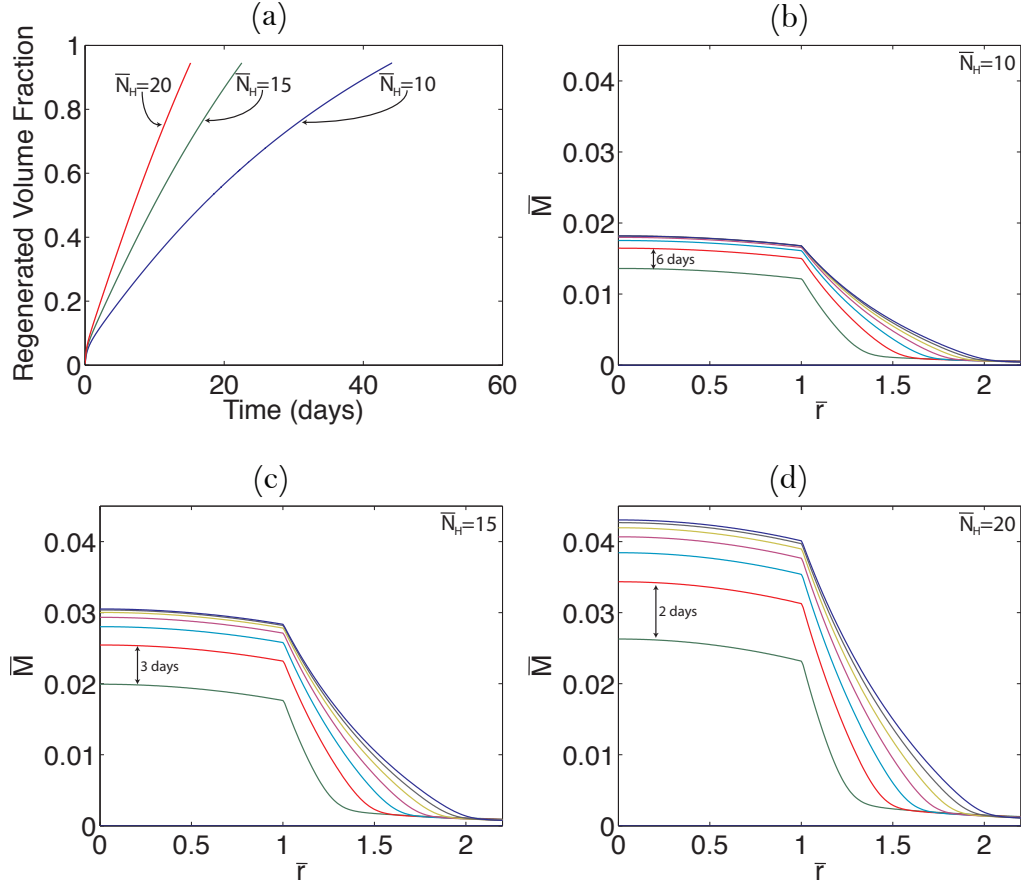
Figure 3.6: (a) A plot of regenerated volume fraction $\tilde{V}_{ECM}(\bar{t})$ for three values of $\bar{N}_H$. (b) The case $\bar{N}_H = 10$, for which $T_{regen} = 44.1$ days. Successive curves advance upwards at intervals of 6 days. (c) The case $\bar{N}_H = 15$, for which $T_{regen} = 22.5$ days. Successive curves advance upwards at intervals of 3 days. (d) The case $\bar{N}_H = 20$, for which $T_{regen} = 15.2$ days. Successive curves advance upwards at intervals of 2 days.
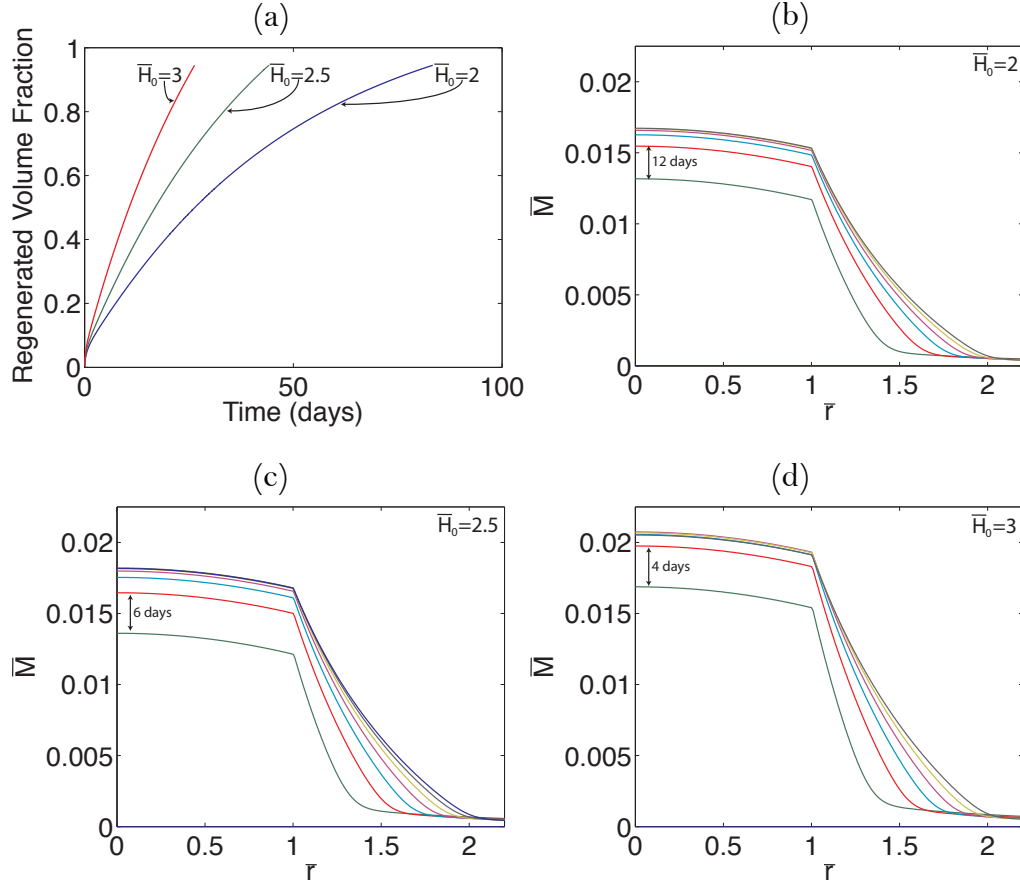
Figure 3.7: (a) A plot of regenerated volume fraction $\tilde{V}_{ECM}(\bar{t})$ for three values of $\bar{H}_0$. (b) The case $\bar{H}_0 = 2$, for which $T_{regen} = 83.4$ days. Successive curves advance upwards at intervals of 12 days. (c) The case $\bar{H}_0 = 2.5$, for which $T_{regen} = 44.1$ days. Successive curves advance upwards at intervals of 6 days. (d) The case $\bar{H}_0 = 3$, for which $T_{regen} = 26.3$ days. Successive curves advance upwards at intervals of 4 days.
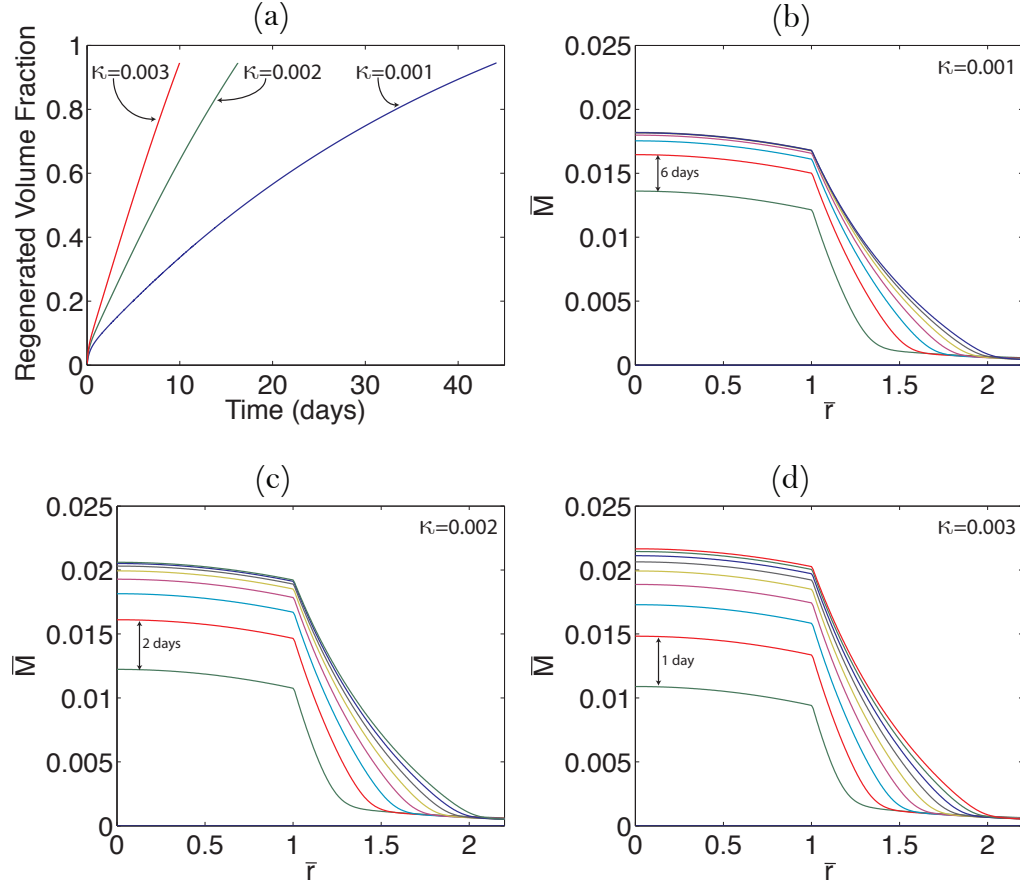
Figure 3.8: (a) A plot of regenerated volume fraction $\tilde{V}_{ECM}(\bar{t})$ for three values of κ. (b) The case $\kappa = 0.001$, for which $T_{regen} = 44.1$ days. Successive curves advance upwards at intervals of 6 days. (c) The case $\kappa = 0.002$, for which $T_{regen} = 16.3$ days. Successive curves advance upwards at intervals of 2 days. (d) The case $\kappa = 0.003$, for which $T_{regen} = 10.0$ days. Successive curves advance upwards at intervals of 1 day.
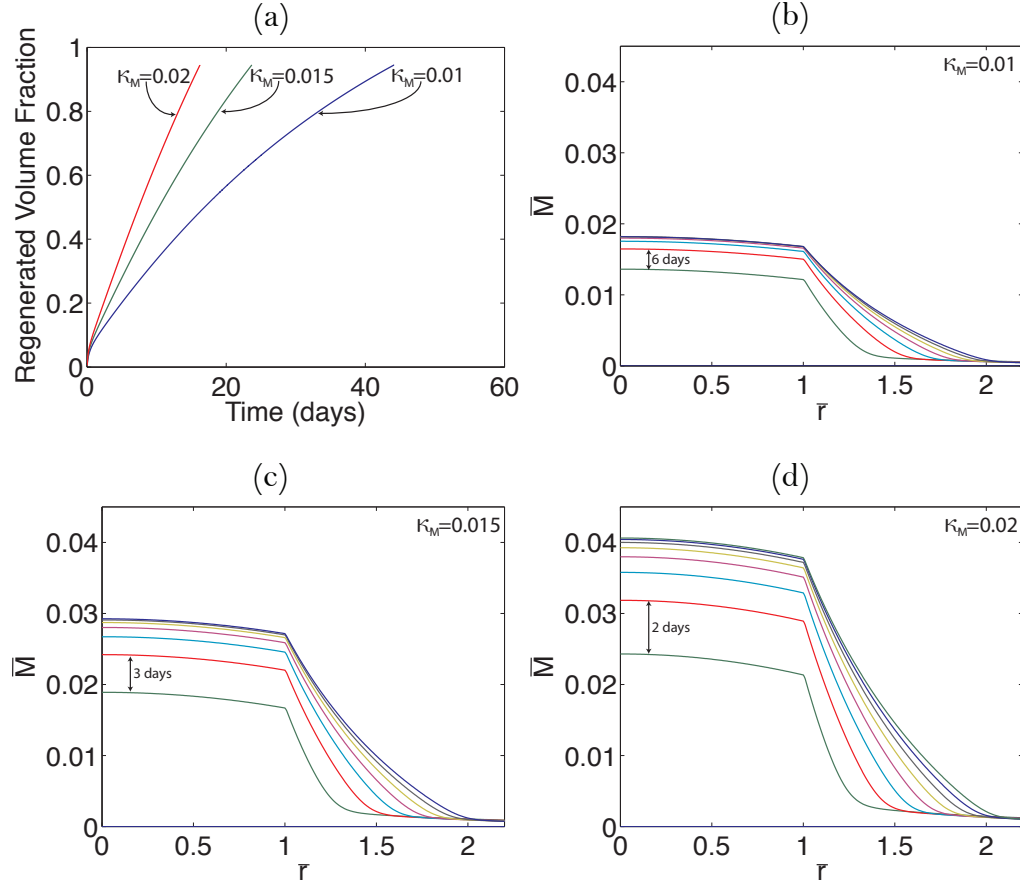
Figure 3.9: (a) A plot of regenerated volume fraction $\tilde{V}_{ECM}(\bar{t})$ for three values of κ_M. (b) The case $\kappa_M = 0.01$, for which $T_{regen} = 44.1$ days. Successive curves advance upwards at intervals of 6 days. (c) The case $\kappa_M = 0.015$, for which $T_{regen} = 23.7$ days. Successive curves advance upwards at intervals of 3 days. (d) The case $\kappa_M = 0.02$, for which $T_{regen} = 16.2$ days. Successive curves advance upwards at intervals of 2 days.

3.4.4   Power Law Relationships

Dependence of the regeneration time, T_{regen}, on several model parameters was also investigated. In Figure 3.10, regeneration times were plotted as points $\left(\bar{N}_H, T_{regen}\right)$ for five values of κ: $\kappa = 0.0005$, $\kappa = 0.00075$, $\kappa = 0.001$, $\kappa = 0.002$, and $\kappa = 0.003$. Power law fits were computed for each κ value, yielding the equations found in Table 3.4, and the solid curves in Figure 3.10.

Similarly, in Figure 3.11, regeneration times are plotted as points (κ, T_{regen}) for five values of $\delta_M^{(3)}$: $\delta_M^{(3)} = 5$, $\delta_M^{(3)} = 10$, $\delta_M^{(3)} = 15$, $\delta_M^{(3)} = 20$, and $\delta_M^{(3)} = 25$. Corresponding power law fits and R^2 values are found in Table 3.5, and are denoted by the solid curves in the figure.

Lastly, in Figure 3.12, regeneration times are plotted as points $\left(\bar{N}_H, T_{regen}\right)$, but this time for the values of $\delta_M^{(3)}$ stated in the previous paragraph. Power law fits and R^2 values were computed and are found in Table 3.6, and are denoted by the solid curves in the figure.

The power law curve fits presented above illustrate how effective responses or outcomes of the cartilage regeneration process can be analyzed. Given the difficulties associated with obtaining detailed spatio-temporal data over the long time scales, such effective relations can aid in quantitatively characterizing controllable parts of the process for optimal biomaterial design of the scaffold. With spatial models such as the one that was developed in this study, similar analysis can be repeated for the specific combination of parameters of interest to the experimentalist.

Table 3.4: Power law fits of regeneration time, T_{regen}, as a function of $\bar{N}_H$ for five values of κ. Corresponding plots are found in Figure 3.10 (R^2 is the coefficient of determination).

Case	κ	$T_{regen}\left(\bar{N}_H; \kappa\right)$	R^2
I	0.0005	$T_{regen} = 12877\left(\bar{N}_H\right)^{-1.91}$	0.995
II	0.00075	$T_{regen} = 4333.7\left(\bar{N}_H\right)^{-1.76}$	0.989
III	0.001	$T_{regen} = 2343\left(\bar{N}_H\right)^{-1.68}$	0.985
IV	0.002	$T_{regen} = 484.51\left(N_H\right)^{-1.43}$	0.989
V	0.003	$T_{regen} = 208.89\left(N_H\right)^{-1.29}$	0.995
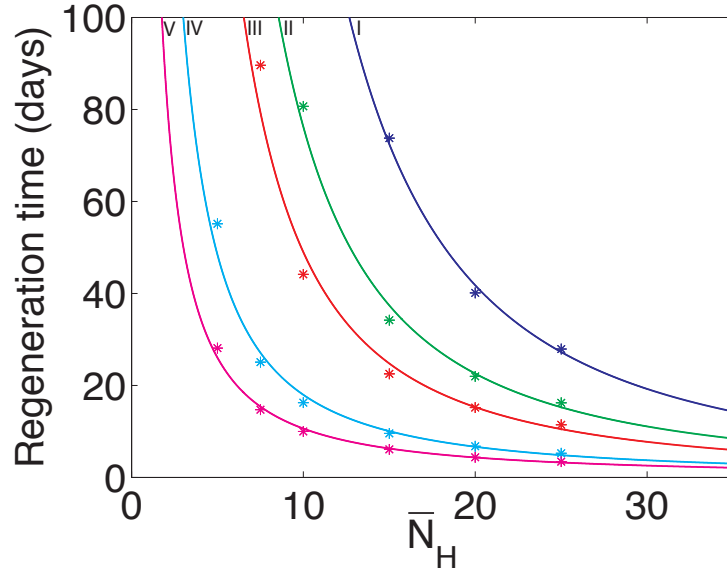
Figure 3.10: Plots of regeneration time, T_{regen}, as a function of $\bar{N}_H$ for five values of κ. Each * represents the regeneration time for a $\left(\bar{N}_H; \kappa\right)$ pair, while the corresponding solid lines represent the power law fits. Equations and R^2 values are found in Table 3.4.

Table 3.5: Power law fits of regeneration time, T_{regen}, as a function of κ for five values of $\delta_M^{(3)}$. Corresponding plots are found in Figure 3.11 (R^2 is the coefficient of determination).

Case	$\delta_M^{(3)}$	$T_{regen}\left(\kappa; \delta_M^{(3)}\right)$	R^2
VI	5	$T_{regen} = 0.0035\kappa^{-1.12}$	0.999
VII	10	$T_{regen} = 0.003\kappa^{-1.26}$	0.995
VIII	15	$T_{regen} = 0.0009\kappa^{-1.53}$	0.972
IX	20	$T_{regen} = 0.0017\kappa^{-1.49}$	0.992
X	25	$T_{regen} = 0.0018\kappa^{-1.52}$	0.996
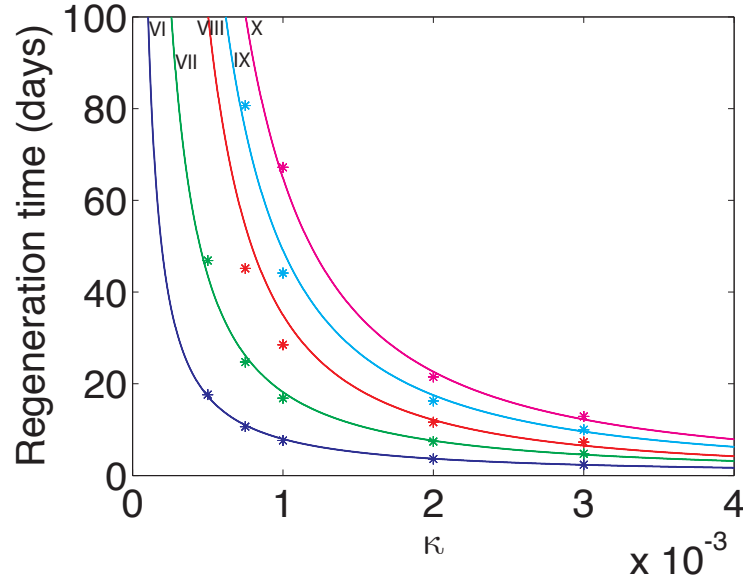
Figure 3.11: Plots of regeneration time, T_{regen}, as a function of κ for five values of $\delta_M^{(3)}$. Each * represents the regeneration time for a $\left(\kappa; \delta_M^{(3)}\right)$ pair, while the corresponding solid lines represent the power law fits. Equations and R^2 values are found in Table 3.5.

Table 3.6: Power law fits of regeneration time, T_{regen}, as a function of $\bar{N}_H$ for five values of $\delta_M^{(3)}$. Corresponding plots are found in Figure 3.12 (R^2 is the coefficient of determination).

Case	$\delta_M^{(3)}$	$T_{regen}\left(\bar{N}_H; \delta_M^{(3)}\right)$	R^2
XI	5	$T_{regen} = 151.5\left(\bar{N}_H\right)^{-1.28}$	0.996
XII	10	$T_{regen} = 592.03\left(\bar{N}_H\right)^{-1.51}$	0.988
XIII	15	$T_{regen} = 841.84\left(\bar{N}_H\right)^{-1.45}$	0.994
XIV	20	$T_{regen} = 2343\left(\bar{N}_H\right)^{-1.68}$	0.985
XV	25	$T_{regen} = 2905.7\left(\bar{N}_H\right)^{-1.66}$	0.992
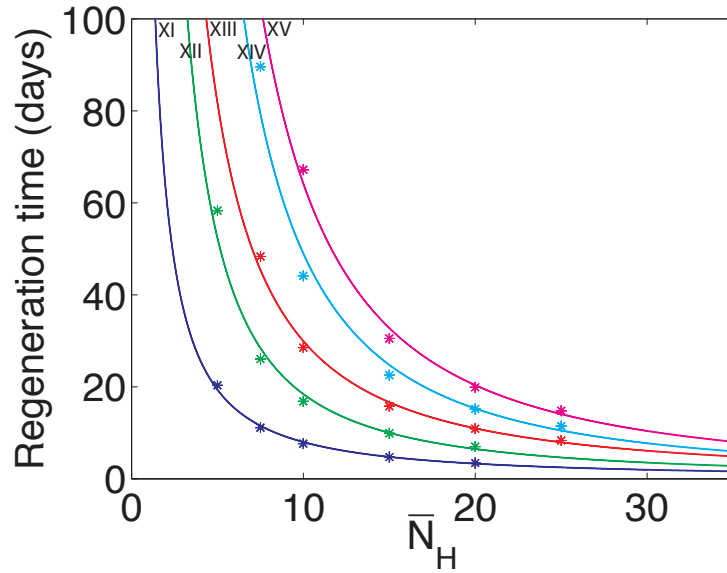
Figure 3.12: Plots of regeneration time, T_{regen}, as a function of $\bar{N}_H$ for five values of $\delta_M^{(3)}$. Each * represents the regeneration time for a $\left(\bar{N}_H; \delta_M^{(3)}\right)$ pair, while the corresponding solid lines represent the power law fits. Equations and R^2 values are found in Table 3.6.

3.5   Reduced Model: Constant Nutrients

It was observed in previous sections that nutrient diffusion occurs on a much faster time scale than the other mechanisms included in the model. Specifically, in Figure 3.3 it was observed that $\bar{N}(\bar{r}, \bar{t})$ remains close to $\bar{N}_H$. A model simplification can be considered in which $\bar{N}$ is taken to be constant, as in (2.65). This eliminates four parameters: the nutrient diffusivities, $\delta_N^{(1)}$, $\delta_N^{(2)}$, $\delta_N^{(3)}$, and the nutrient absorption rate, κ_N.

The resulting changes in regeneration time for the original and simplified models are essentially negligible in the nondimensional time domain. Differences are on the order of only a few hours, with the largest being for the case where $\bar{H}_0 = 2$ resulting in a change in regeneration time from 83.41 days in the original model to 83.17 days in the reduced model - a difference of less than 6 hours. Differences were larger for greater regeneration times, but the percent difference stayed consistently less than 0.5%. Comparisons were made for all of the parameter values studied in Section 3.4, and can be found in Table 3.7. Spatial profiles are close to identical to those of the original model, and therefore are not reproduced here.

Based on these findings, the reduced model could serve as an accurate simplification of the original model, and has the advantages of containing fewer parameters and being less computationally intensive. The simplified model still incorporates the effects of nutrient concentration via the parameter $\bar{N}_H$, but since nutrient-related phenomena occurred on such comparatively fast time scales, the subtle spatial differences in nutrient concentration have a negligible effect on the end result for calculation of ECM regeneration times.

Table 3.7: Comparison of regeneration times from the original model, T_{regen}, and the reduced case where $\bar{N}(\bar{r}, \bar{t}) \equiv \bar{N}_H$, denoted as $\hat{T}_{regen}$. The percent difference was consistently far less than 0.5% and the largest change was less than 6 hours.

Changing Parameter	Value	T_{regen}	$\hat{T}_{regen}$	Change	% Difference
–	–	44.13 days	44.04 days	2 hrs, 10 min	0.20%
$\bar{N}_H$	15	22.53 days	22.49 days	58 min	0.18%
$\bar{N}_H$	20	15.17 days	15.15 days	29 min	0.13%
$\bar{H}_0$	2	83.41 days	83.17 days	5 hr, 46 min	0.29%
$\bar{H}_0$	3	26.35 days	26.29 days	1 hr, 26 min	0.23%
$\delta_M^{(3)}$	15	28.51 days	28.46 days	1 hr, 12 min	0.18%
$\delta_M^{(3)}$	25	67.19 days	67.01 days	4 hr, 19 min	0.27%
κ	0.002	16.27 days	16.24 days	43 min	0.18%
κ	0.003	9.98 days	9.96 days	29 min	0.20%
κ_M	0.015	23.69 days	23.64 days	1 hr, 12 min	0.21%
κ_M	0.02	16.23 days	16.20 days	43 min	0.18%

3.6   Summary

The reaction-diffusion models presented in this study have proven able to capture many of the important biophysical, physiological, and scaffold-design aspects of cartilage regeneration. In the context of hydrogel scaffolds seeded with chondrocytes, they can provide a framework for quantitative characterization of hydrogel biomaterial design. Developing such a framework is important because the associated experiments can be costly and time-intensive; using mathematical models could streamline the hydrogel-design process, making it more effective and efficient.

While, in this model, it was determined that the availability of excess nutrients is crucial, and that increasing the nutrient level significantly decreases the regeneration time, the subtle spatial differences in nutrient concentration due to diffusion and absorption do not play a major role in tissue regeneration. Approximating the reaction-diffusion models for nutrient concentration with a constant function had a negligible effect on the end result for overall ECM regeneration times (only a few hours difference, in dimensional time).

Chapter 4

A Phenomenological Approach to Modeling Cartilage Regeneration

4.1 Introduction

While partial differential equation models such as the reaction-diffusion model developed and discussed in Chapters 2 and 3 are useful in terms of their direct relevance to biophysical and biomechanical processes involved in tissue engineering, an argument can be made for the development of more phenomenological ordinary differential equation models. While only a few ODE models have been published (see Section 1.4.2), there are many challenges to the experimentalist in obtaining adequate spatial data sets over the lengthy time scales associated with cartilage regeneration. Consequently, experimental data in most studies tends to be purely temporal, and PDE model results are typically spatially averaged in order to validate against this data. In this chapter, the concept of directly analyzing cartilage regeneration via a temporal model is investigated, motivated by its clear advanatages with respect to efficiency and simplicity relative to the spatio-temporal models.

Wilson et al. [38] developed models for scaffold degradation, ECM production (delineating between GAG and collagen), and the resulting total mass of the tissue construct. Scaffold degradation and ECM production were assumed to be indepen-

dent processes, dependent only on the remaining mass of each quantity,

$$\frac{d[\text{ECM}]}{dt} = k_{\text{ECM}}([\text{ECM}]_{SS} - [\text{ECM}]), \qquad (4.1)$$

$$\frac{d[\text{Scaffold}]}{dt} = -k_{\text{Scaffold}}[\text{Scaffold}]. \qquad (4.2)$$

This linear uncoupled model is highly advantageous because its simplicity yields the analytical solution

$$[\text{ECM}](t) = [\text{ECM}]_{SS}\left(1 - e^{-t/\tau_{\text{ECM}}}\right), \qquad (4.3)$$

$$[\text{Scaffold}](t) = [\text{Scaffold}]_0 e^{-t/\tau_{\text{Scaffold}}}, \qquad (4.4)$$

where $[\text{Scaffold}]_0$ is the initial scaffold mass, $[\text{ECM}]_{SS}$ is the steady state ECM concentration, and $\tau_{\text{Scaffold}} = 1/k_{\text{Scaffold}}$ and $\tau_{\text{ECM}} = 1/k_{\text{ECM}}$ are characteristic time constants. Lastly, Wilson et al. described the total mass, $M(t)$, of the construct as the sum of its constituent masses as,

$$\begin{aligned} M(t) = {} & \text{cell mass} + [\text{GAG}]_{SS}\left(1 - e^{-t/\tau_{\text{GAG}}}\right) \\ & + [\text{Collagen}]_{SS}\left(1 - e^{-t/\tau_{\text{Collagen}}}\right) \\ & + [\text{Scaffold}]_0 e^{-t/\tau_{\text{Scaffold}}} \end{aligned} \qquad (4.5)$$

These models were then validated against multiple sets of data by curve-fitting. Although the models were simple, they fit quite well to the data [38]. Some of the assumptions, however, could be neglecting potentially important interaction mechanisms in the tissue regeneration process.

The regeneration rate and structural integrity of the tissue depend on the rate of hydrogel degradation: if the scaffold degrades too quickly, defects could appear, while if it degrades too slowly it could inhibit tissue growth by preventing timely distribution and linking of the ECM molecules [29]. Obradovic et al. [24] observed that matrix synthesis depends on both the availability of nutrients and some regulatory feedback mechanism. In this chapter, the Wilson et al. [38] model is extended to delineate ECM into its "unlinked" (soluble, unbound, diffusing) and "linked" (bound, non-diffusing) constituents, and to capture the coupled nature of the relationships between the hydrogel scaffold, matrix, and nutrients.

4.2 Model Development

In the model to be considered, there are six dependent variables: intracellular nutrient level, matrix (separated into unlinked collagen, unlinked GAG, linked collagen, and linked GAG), and scaffold. For consistency with the experimental data to be considered in this chapter, all variables except for the nutrient level are measured as dry mass. The nutrients and unlinked matrix are diffusing molecules, while the other three dependent variables are bound.

4.2.1 Nutrient Absorption and Utilization

The intracellular nutrient level, $N = N(t)$, can be modeled by an equation of the form

$$\frac{dN}{dt} = f_1(S)\left(M_* - M_L^C - M_L^G\right) - g(N), \tag{4.6}$$

where S is the mass of scaffold material, and M_L^C and M_L^G are the masses of linked collagen and GAG, respectively. The parameter M_* is the steady-state total linked ECM dry mass and is the sum of steady-state values for both collagen and GAG. The first term on the right hand side of (4.6) models the inhibitory mechanism that slows nutrient absorption within the cell as ECM accumulates in the extracellular environment, and is motivated by the work of Wilson et al. [38], particularly (4.1). As the scaffold degrades, it is assumed that nutrient absorption is enhanced due to increased diffusivity, and we model $f_1(S)$ as a linear decreasing function,

$$f_1(S) = d_1\left(S_* - S\right). \tag{4.7}$$

The parameter S_* is a saturation value intrinsic to the hydrogel design that signifies a point at which the hydrogel scaffold can no longer sustain additional nutrients. The $g(N)$ term in (4.6) models that rate at which excess nutrients are utilized by the chondrocytes, and is modeled by

$$g(N) = c_1\left(N - N_*\right). \tag{4.8}$$

This algebraic form is motivated by the reaction-diffusion model from Chapters 2 and 3, and particularly by the intracellular nutrient concentration equation, (2.3), where N_* represents the homeostatic nutrient level.

4.2.2 Matrix Synthesis and Linking: Collagen and GAG

The unlinked collagen and GAG, or $M_U^C = M_U^C(t)$ and $M_U^G = M_U^G(t)$, respectively, are modeled by equations of the form

$$
\begin{aligned}
\frac{dM_U^C}{dt} &= f_2(N)\left(M_* - M_L^C - M_L^G\right) - k_C M_U^C S, & (4.9) \\
\frac{dM_U^G}{dt} &= f_3(N)\left(M_* - M_L^C - M_L^G\right) - k_G M_U^G S. & (4.10)
\end{aligned}
$$

The first term on the right hand side of both (4.9) and (4.10) models the regulatory feedback mechanism of a chondrocyte's ability to synthesize matrix. Just as in (4.6) and (4.1), as the ECM accumulates in the extracellular environment, cell regulated biosynthesis of unlinked ECM constituents is inhibited. Also, unlinked matrix synthesis has been shown to increase with increasing intracellular nutrient levels, hence the terms $f_2(N)$ and $f_3(N)$ are modeled by

$$
\begin{aligned}
f_2(N) &= d_2\left(N - N_*\right), & (4.11) \\
f_3(N) &= d_3\left(N - N_*\right). & (4.12)
\end{aligned}
$$

The second term on the right hand side in both (4.9) and (4.10) models the binding of unlinked matrix with the scaffold in the ECM linking process. When unlinked collagen or GAG bind with the scaffold, they are essentially taken out of the system and become linked. This process is modeled by the equations

$$
\begin{aligned}
\frac{dM_L^C}{dt} &= k_C M_U^C S, & (4.13) \\
\frac{dM_L^G}{dt} &= k_G M_U^G S. & (4.14)
\end{aligned}
$$

4.2.3   Scaffold Degradation

Scaffold is not created during the cartilage regeneration process; it degrades due to the binding process described above, and other inherent degradation mechanisms independent of the ECM and intracellular nutrient levels. Scaffold degradation is modeled by

$$\frac{dS}{dt} = -l_C M_U^C S - l_G M_U^G S - c_2 S, \tag{4.15}$$

where $l_C < k_C$ and $l_G < k_G$. The first two terms take the same form as (4.13) and (4.14), but these two degradation rate constants are smaller because it is assumed that degradation due to linking is slower than the linking process itself. The third term results from the scaffold's inherent degradation rate and is motivated by (4.2).

4.2.4   Initial Conditions

The initial conditions for this model are analagous to (2.15)-(2.17). Initially, the chondrocyte contains a homeostatic level of nutrients,

$$N(0) = N_*, \tag{4.16}$$

there is no unlinked or linked matrix present in the system,

$$M_U^C(0) = 0, \qquad\qquad M_U^G(0) = 0, \tag{4.17}$$

$$M_L^C(0) = 0, \qquad\qquad M_L^G(0) = 0, \tag{4.18}$$

and the initial scaffold mass is known,

$$S(0) = S_0. \tag{4.19}$$

4.2.5 Cartilage Regeneration Model

The cartilage regeneration model then consists of the governing equations

$$\frac{dN}{dt} = d_1 \left(S_* - S \right) \left(M_* - M_L^C - M_L^G \right) - c_1 \left(N - N_* \right), \tag{4.20}$$

$$\frac{dM_U^C}{dt} = d_2 \left(N - N_* \right) \left(M_* - M_L^C - M_L^G \right) - k_C M_U^C S, \tag{4.21}$$

$$\frac{dM_U^G}{dt} = d_3 \left(N - N_* \right) \left(M_* - M_L^C - M_L^G \right) - k_G M_U^G S, \tag{4.22}$$

$$\frac{dM_L^C}{dt} = k_C M_U^C S, \tag{4.23}$$

$$\frac{dM_L^G}{dt} = k_G M_U^G S, \tag{4.24}$$

$$\frac{dS}{dt} = -l_C M_U^C S - l_G M_U^G S - c_2 S, \tag{4.25}$$

subject to the conditions (4.16)-(4.19).

4.2.6 Steady State Analysis

The steady states of the model in (4.20)-(4.25) in the limit as $t \to \infty$ were analyzed. In the scaffold equation (4.25), observe that at steady state, $S = 0$ or $c_2 = -l_C M_U^C - l_G M_U^G$. Since c_2, l_C, l_G are all nonnegative parameters and $M_U^C(t) \geq 0$ and $M_U^G(t) \geq 0$ for $t \geq 0$, it follows that $S = 0$ at steady state. Using this result and (4.21)-(4.22) it is observed that $N = N_*$ or $M_L^C + M_L^G = M_*$. From (4.20), using the fact that $f_1(0) = S_* > 0$ at steady state, it is observed that both of these conditions must be true. In summary, in the limit as $t \to \infty$,

$$N = N_*, \tag{4.26}$$

$$M_L^C + M_L^G = M_*, \tag{4.27}$$

$$S = 0, \tag{4.28}$$

meaning that the intracellular nutrient level returns to homeostasis, the amount of linked ECM has reached its target amount, and the scaffold has fully degraded. Note that M_U^C and M_U^G are free to remain at constant levels in the system. While it is

difficult to assess the accuracy of this steady state property, it arises in our model since the regulation of cellular biosynthesis of ECM constituents is determined by the mass of linked matrix in the system. Since unlinked matrix is an intermediate species in our model, it is also assumed that unlinked matrix mass will be small relative to scaffold and linked matrix mass as the cartilage regeneration process progresses.

4.3   Model Calibration

The model was calibrated using experimental data from the Wilson et al. [38] study. In this study, data was provided for means values of the dry mass of scaffold, as well as the percent dry mass of GAG and collagen. The percent dry mass GAG at time t, $G(t)$, is computed by

$$G(t) \;=\; \frac{M_U^G(t) + M_L^G(t)}{\text{Mass(t)}} \times 100, \tag{4.29}$$

where the total mass in the cell-biomaterial system is given by

$$\text{Mass}\,(t) \;=\; \text{cell mass} \;+\; \underbrace{M_U^G(t) + M_L^G(t)}_{\text{GAG}} + \underbrace{M_U^C(t) + +M_L^C(t)}_{\text{Collagen}} + S(t). \tag{4.30}$$

The percent dry mass collagen, $C(t)$, is computed similarly by

$$C(t) \;=\; \frac{M_U^C(t) + M_L^C(t)}{\text{Mass(t)}} \times 100. \tag{4.31}$$

Note that the mass contribution due to the nutrients is considered negligible. Wilson et al. reported a constant cell mass value of 0.21 mg, and an initial scaffold dry mass of $S_0 = 18.04$ mg [38].

To aid in fitting the experimental data to the current model, a least squares cost function was formulated. The cost, J, for a set of parameters, q, is given by

$$J(q) \;=\; \frac{1}{n_S} \sum_{i=1}^{n_S} \left(\frac{\hat{S}_i - S(t_i; q)}{\max\left\{ \hat{S}_i \right\}} \right)^2 + \frac{1}{n_G} \sum_{i=1}^{n_G} \left(\frac{\hat{G}_i - G(t_i; q)}{\max\left\{ \hat{G}_i \right\}} \right)^2$$

$$+ \frac{1}{n_C} \sum_{i=1}^{n_C} \left(\frac{\hat{C}_i - C(t_i; q)}{\max\left\{ \hat{C}_i \right\}} \right)^2, \tag{4.32}$$

where n_S is the number of scaffold data points $\hat{S}_i$, and n_G, $\hat{G}_i$, n_C, and $\hat{C}_i$ are defined analogously. In this case, the number of data points are equal; that is,

$$n = n_S = n_G = n_C, \tag{4.33}$$

and (4.32) becomes

$$J(q) \;=\; \frac{1}{n}\sum_{i=1}^{n}\left[\left(\frac{\hat{S}_i - S(t_i;q)}{\max\left\{\hat{S}_i\right\}}\right)^2 + \left(\frac{\hat{G}_i - G(t_i;q)}{\max\left\{\hat{G}_i\right\}}\right)^2 + \left(\frac{\hat{C}_i - C(t_i;q)}{\max\left\{\hat{C}_i\right\}}\right)^2\right] \tag{4.34}$$

For a fixed set of parameter values, q, solutions to equations (4.20)-(4.25) subject to initial conditions (4.16)-(4.19) are approximated using the MATLAB routine `ode15s`. Optimization of the cost function was done with the MATLAB routine `fminsearch`, a Nelder-Meader direct search simplex method [20].

Without loss of generality, the intracellular nutrient level variable was normalized so that $N_* = 1$. Taking into consideration the constraints $S_* > S_0$, $l_C < k_C$, and $l_G < k_G$, the initial parameter estimates for use in the optimization routine were set at

$$d_1 = 0.1, \qquad d_2 = 0.1, \qquad d_3 = 0.1, \tag{4.35}$$

$$M_* = 1, \qquad S_* = 2S_0, \qquad c_1 = 0.1, \qquad c_2 = 0.1, \tag{4.36}$$

$$k_C = 0.1, \qquad k_G = 0.1, \qquad l_C = k_C/3, \qquad l_G = k_G/3. \tag{4.37}$$

The resulting optimal parameter values are shown in Table 4.3, and the corresponding cost function value and coefficients of determination for the scaffold, collagen, and GAG are shown in Table 4.3.

In Figure 4.1, solutions to this model for the parameters in Table 4.3 are shown. Note that the intracellular nutrient level peaks early, and around the same time the linked ECM reaches its target value, M_*. The unlinked matrix also peaks early, and is completely converted to linked ECM by the time target ECM is reached. The excess nutrients in the system are removed on a slower scale, but return to homeostasis eventually. Overall, the scaffold degradation occurs on the slowest scale. It should

also be noted that there are features of the data (represented by the red dots in the Figure 4.1(d)-(f)) that don't appear to be captured by the ODE model. It is unclear whether these are inaccuracies associated with the experimental procedure, the simplicity of the model, or a combination of both. In particular, the behavior of the model around the 30 day mark in plots (d) and (f) plots differ noticeably from the data. Since, at this point in the process, all variables other that $S(t)$ are near steady-state, there could be an additional mechanism involved in the scaffold degradation that has been neglected in the current model.

Table 4.1: Parameter values and corresponding units resulting from minimizing the cost function, J, subject to the initial parameter estimates.

c_1	c_2	d_1	d_2	d_3	k_C	k_G	l_C	l_G	M_*	S_*
0.164	0.027	0.155	0.136	0.034	0.101	0.110	0.026	0.052	0.381	49.3
s^{-1}	s^{-1}	$mg^{-2}s^{-1}$	s^{-1}	s^{-1}	$mg^{-1}s^{-1}$	$mg^{-1}s^{-1}$	$mg^{-1}s^{-1}$	$mg^{-1}s^{-1}$	mg	mg

Table 4.2: Resulting minimum value of the cost function, J, subject to the initial parameter estimates, and coefficient of determination, R^2, for each data set.

J	$R^2_{Scaffold}$	$R^2_{Collagen}$	R^2_{GAG}
0.059	0.891	0.758	0.948

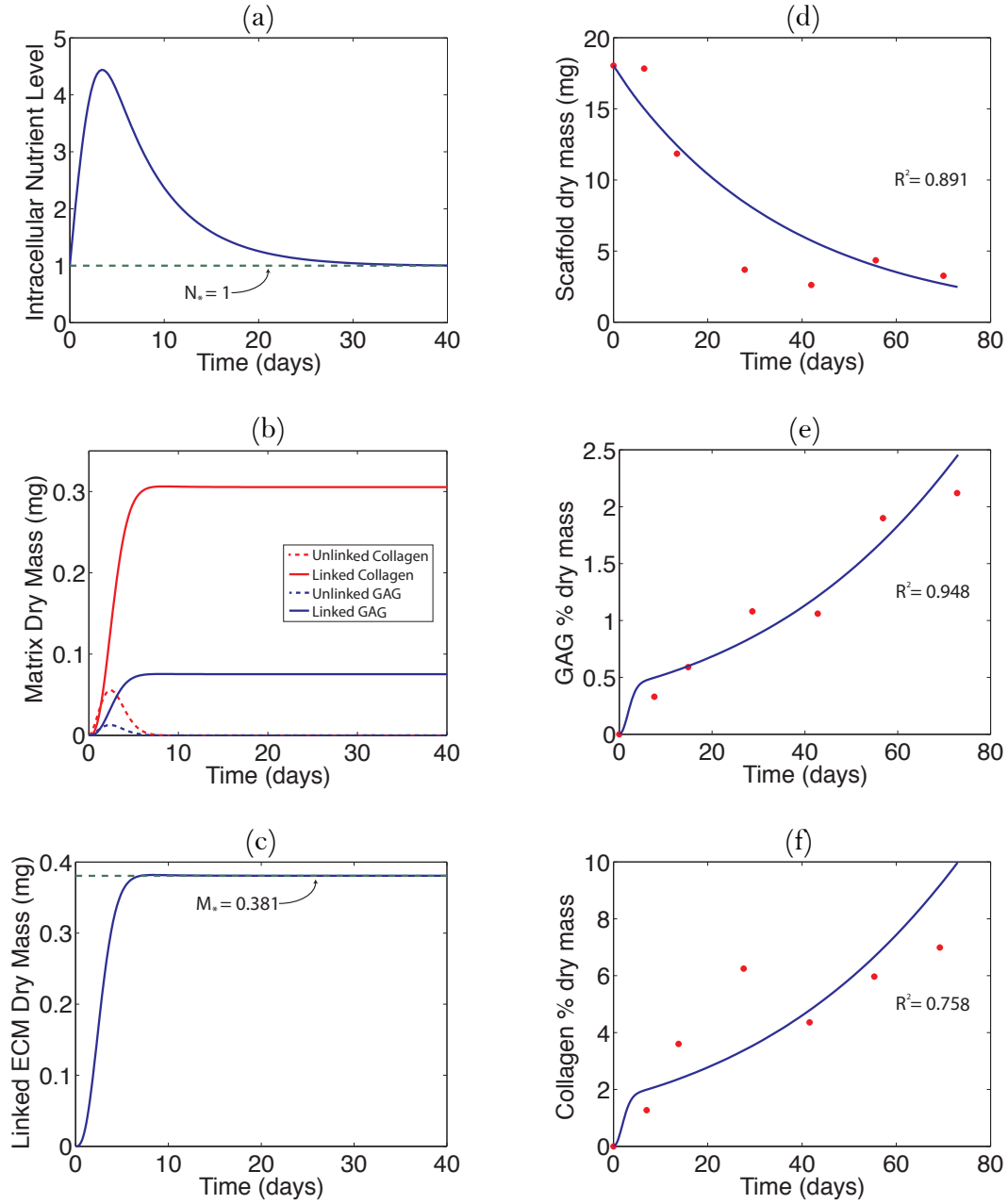Figure 4.1: Model variables for the case of optimal parameter values of Table 4.3 (a) intracellular nutrient level, $N(t)$, (b) dry mass of unlinked and linked collagen and GAG, and (c) total linked ECM (collagen and GAG) dry mass. Results of least squares fit (blue line) to the Wilson et al. [38] data (red dots) and corresponding R^2 values for (d) scaffold dry mass, (e) GAG % dry mass, and (f) collagen % dry mass.

4.4 Parametric Analysis

Just as in Section 3.4 with the PDE model, a parametric analysis was conducted in terms of a regeneration time, T_{regen}. As there is no characteristic volume for this model, T_{regen} was computed as the time at which the total linked ECM dry mass first exceeds 95% of the target value, or

$$\min \left\{ T_{regen} : M_L^C(T_{regen}) + M_L^G(T_{regen}) \geq 0.95 M_* \right\}. \tag{4.38}$$

4.4.1 Scaffold Properties

In the Wilson et al. [38] experiment, the large majority of the dry mass was made up of the scaffold. Therefore it seems of significant interest to investigate the impact of changes in the initial scaffold mass, S_0, or the scaffold saturation value, S_*, on the model responses and regeneration time. Solutions to the model were found for equally spaced values of S_0 and S_*. Three S_0 values,

$$S_0 = 0.6(18.04) = 10.82 \text{ mg}, \quad S_0 = 18.04 \text{ mg}, \quad S_0 = 1.4(18.04) = 25.26 \text{ mg}, \tag{4.39}$$

were considered, and results are shown in Figure 4.2.

In Figure 4.2(a), observe that increasing the initial scaffold mass also increases the regeneration time. For $S_0 < 10$, however, the regeneration times seem to increase as S_0 decreases. It is unclear whether this is due to more complex interactions, or is a weakness in that the model is producing unrealistic responses in some parameter ranges. In particular, in Figure 4.2(b) the intracellular nutrient level drops below its homeostasic level. It was stated previously that Rice and Anseth [29] found that the rate and integrity of the regenerated ECM depends on the rate of scaffold degradation: if the scaffold degrades too quickly, defects could appear, while if it degrades too slowly it could inhibit tissue growth by preventing timely distribution of the ECM molecules. It follow that if the experiment begins with too little scaffold, it could have a similar effect to fast degradation, and the chondrocytes could suffer as a result.

It is also observed that for early time, a greater initial scaffold mass results in a lower peak intracellular nutrient level. This could be due to inhibited diffusion

through the scaffold. In Figure 4.2(c), the total linked ECM dry mass is shown (i.e. $M_L^C(t) + M_L^G(t)$). In each of the three cases, the steady-state value of M_* is reached, but at a slower rate for the cases of greater scaffold mass. This also appears to be due to inhibited diffusion.

In examining the scaffold saturation parameter, the values

$$S_* = 0.8(49.30) = 39.44 \text{ mg}, \quad S_* = 49.30 \text{ mg}, \quad S_* = 1.2(49.30) = 59.16 \text{ mg}. \quad (4.40)$$

were studied. In Figure 4.3(a), observe that increasing S_* decreases the regeneration time. This has a similar impact to decreasing S_0, since initial activity is largely determined by the term $(S_* - S_0)$ in (4.20). In 4.3(b)-(c) this effect is also observed; increasing the scaffold saturation value increases the peak intracellular nutrient level, just as it did when the initial scaffold mass was decreased, and it causes the target linked ECM level to be reached faster. Scaffold degradation, shown in Figure 4.3(d), is not significantly affected by changes in S_*.

4.4.2 Binding and Degradation Rates

The binding and degradation parameters, k_C, k_G, l_C, and l_G, control the terms representing the interactions between the unlinked matrix, linked matrix, and scaffold. Varying these parameters between 20% and 240% of the values shown in Table 4.3 had a negligible effect on the regeneration time, as is shown in Figure 4.4. The parameters were also varied as groups: binding rates (k_C, k_G), degradation rates (l_C, l_G), collagen rates (k_C, l_C) and GAG rates (k_G, l_G), but the change in regeneration time was still small. It is noted that all model terms containing these parameters involve the unlinked matrix variables. Based on Figure 4.1, it is evident that these intermediate (unlinked) species become negligible on early time scales. Consequently, their effect on overall regeneration times for linked ECM is less significant relative to other model parameters.

4.4.3 Physiological Parameters

The target linked ECM dry mass, M_*, can contribute to large changes in the regeneration time. It was varied between 20% and 240% of the Table 4.3 value, and the values

$$M_* = 0.4(0.38) = 0.15 \text{ mg}, \quad M_* = 0.38 \text{ mg}, \quad M_* = 1.6(0.15) = 0.61 \text{ mg}, \quad (4.41)$$

were considered, as is shown in Figure 4.5. Due to its presence in (4.20), increasing M_* increases the peak intracellular nutrient level, as shown in Figure 4.5(b). Increasing M_* also appears to accelerate matrix synthesis, allowing linking to happen faster and decreasing the regeneration time. This effect is seen in Figures 4.5(a) and (c). Changes in M_* also have a negligible effect on scaffold degradation.

The parameter d_1 can be interpreted as the intracellular nutrient mobilization rate, and appears in (4.20). Varying d_1 by the same percentages as M_*, above, results in a similar effect on regeneration time and nutrient levels, as seen in Figure 4.6(a) and (b). Increasing d_1 also results in a greater linked ECM dry mass (c), but has no discernible impact on scaffold degradation (d).

The parameter c_1 also appears in (4.20), and describes the rate at which excess nutrients are utilized by the chondrocyte to maintain the integrity of the ECM, and helps the cell return to homeostasis. Increasing c_1 results in a greater regeneration time, as shown in Figure 4.7(a), as the cell expends more nutrients in the biosynthesis of ECM constituents. Decreasing it greatly increases the intracellular nutrient level for later time, as shown in 4.7(b). This has a weaker effect on linked ECM mass (c), however, since the target linked ECM level is reached early, and these additional (unused) nutrients are no longer needed for matrix synthesis. In this case the effects on scaffold mass (d) are negligible.

The parameters d_2 and d_3 are interpreted similarly: they describe the rate at which the chondrocyte uses nutrients to synthesize unlinked collagen and GAG (respectively) in (4.21) and (4.22). It is shown in Figure 4.8(a) that increasing d_2 results in faster tissue regeneration. Since unlinked matrix is synthesized faster for greater d_2, the chondrocyte mobilizes fewer nutrients (b). As observed earlier, increased un-

linked matrix synthesis allows for faster development of linked ECM (c). Varying d_3 results in similar behavior, but to a far lesser degree, as shown in Figure 4.9. This is most likely due to GAG making up a smaller percentage of the total mass in the data used to calibrate the model. Once again, neither of these parameters have a noticeable effect on on scaffold degradation (Figure 4.8(d) and 4.9(d)).

The inherent scaffold degradation rate, c_2, was also studied. As shown in Figure 4.10(a)-(c), even large variations in c_2 had little to no effect on regeneration time, intracellular nutrient level, and linked ECM mass. Smaller values of c_2, as would be expected, do result in slower scaffold degradation (d). Because the scaffold makes up the majority of the total construct mass, this will have a large effect on the percent dry mass, $G(t)$ and $C(t)$, (4.29) and (4.31), that were used when fitting to the data.

Figure 4.2: (a) A plot of regeneration times for different values of S_0 found by varying the optimal parameters found previously. For the three cases denoted by the yellow/blue circles ($S_0 = 10.82$ mg, $S_0 = 18.04$ mg, and $S_0 = 25.26$ mg) plots of (b) intracellular nutrient level, (c) total linked ECM dry mass, and (d) scaffold dry mass are shown.

Figure 4.3: (a) A plot of regeneration times for different values of S_* found by varying the optimal parameters found previously. For the three cases denoted by the yellow/blue circles ($S_* = 39.44$ mg, $S_* = 49.30$ mg, and $S_* = 59.16$ mg) plots of (b) intracellular nutrient level, (c) total linked ECM dry mass, and (d) scaffold dry mass are shown.

Figure 4.4: Plots of regeneration times for different values of the parameters (a) k_C, (b) k_G, (c) l_C, and (d) l_G.

Figure 4.5: (a) A plot of regeneration times for different values of M_* found by varying the optimal parameters found previously. For the three cases denoted by the yellow/blue circles ($M_* = 0.15$ mg, $M_* = 0.38$ mg, and $M_* = 0.61$ mg) plots of (b) intracellular nutrient level, (c) total linked ECM dry mass, and (d) scaffold dry mass are shown.
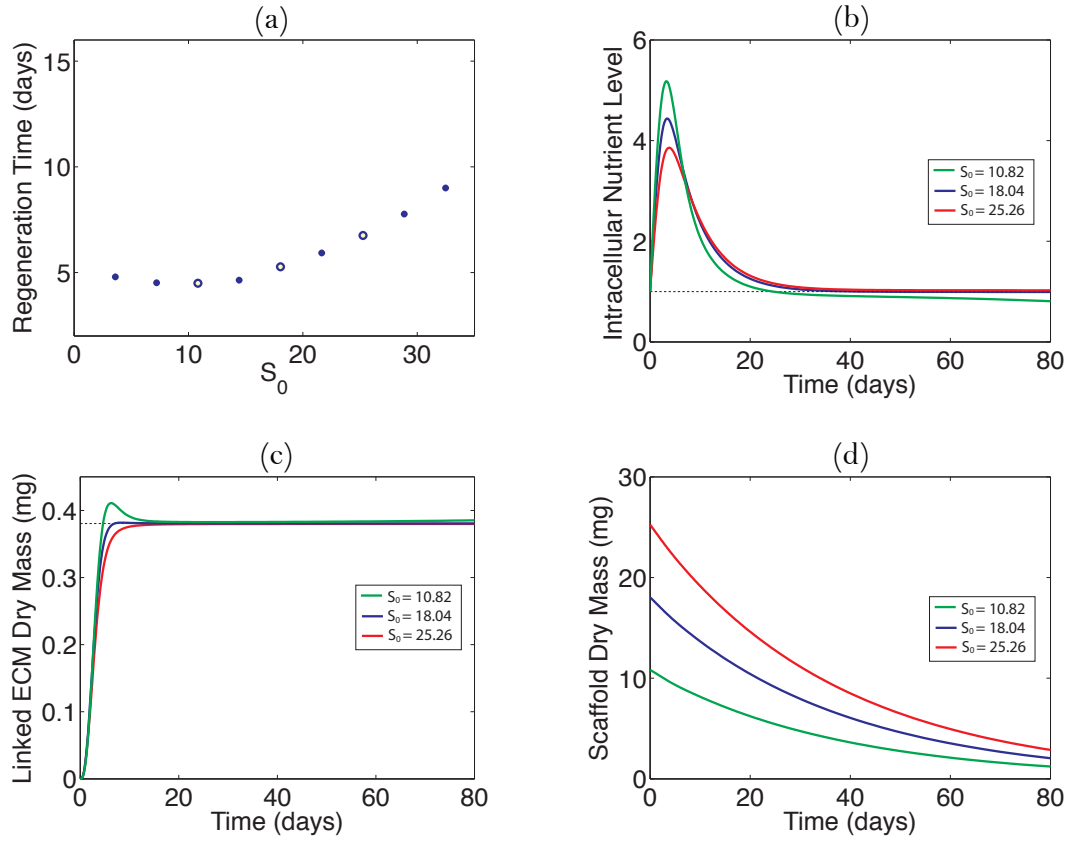
Figure 4.6: (a) A plot of regeneration times for different values of d_1 found by varying the optimal parameters found previously. For the three cases denoted by the yellow/blue circles ($d_1 = 0.06$ mg^{-2}s^{-1}, $d_1 = 0.15$ mg^{-2}s^{-1}, and $d_1 = 0.25$ mg^{-2}s^{-1}) plots of (b) intracellular nutrient level, (c) total linked ECM dry mass, and (d) scaffold dry mass are shown.
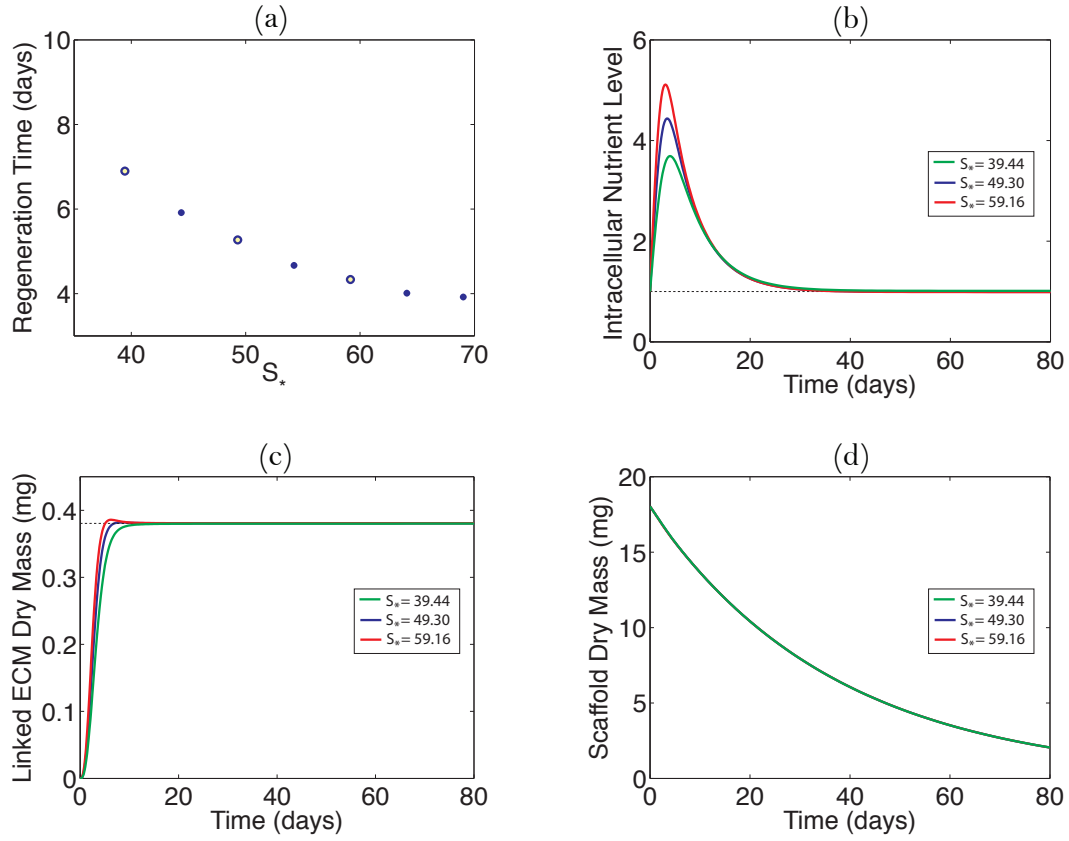
Figure 4.7: (a) A plot of regeneration times for different values of c_1 found by varying the optimal parameters found previously. For the three cases denoted by the yellow/blue circles ($c_1 = 0.03$ s^{-1}, $c_1 = 0.16$ s^{-1}, and $c_1 = 0.30$ s^{-1}) plots of (b) intracellular nutrient level, (c) total linked ECM dry mass, and (d) scaffold dry mass are shown.

Figure 4.8: (a) A plot of regeneration times for different values of d_2 found by varying the optimal parameters found previously. For the three cases denoted by the yellow/blue circles ($d_2 = 0.05$ s^{-1}, $d_2 = 0.14$ s^{-1}, and $d_2 = 0.22$ s^{-1}) plots of (b) intracellular nutrient level, (c) total linked ECM dry mass, and (d) scaffold dry mass are shown.

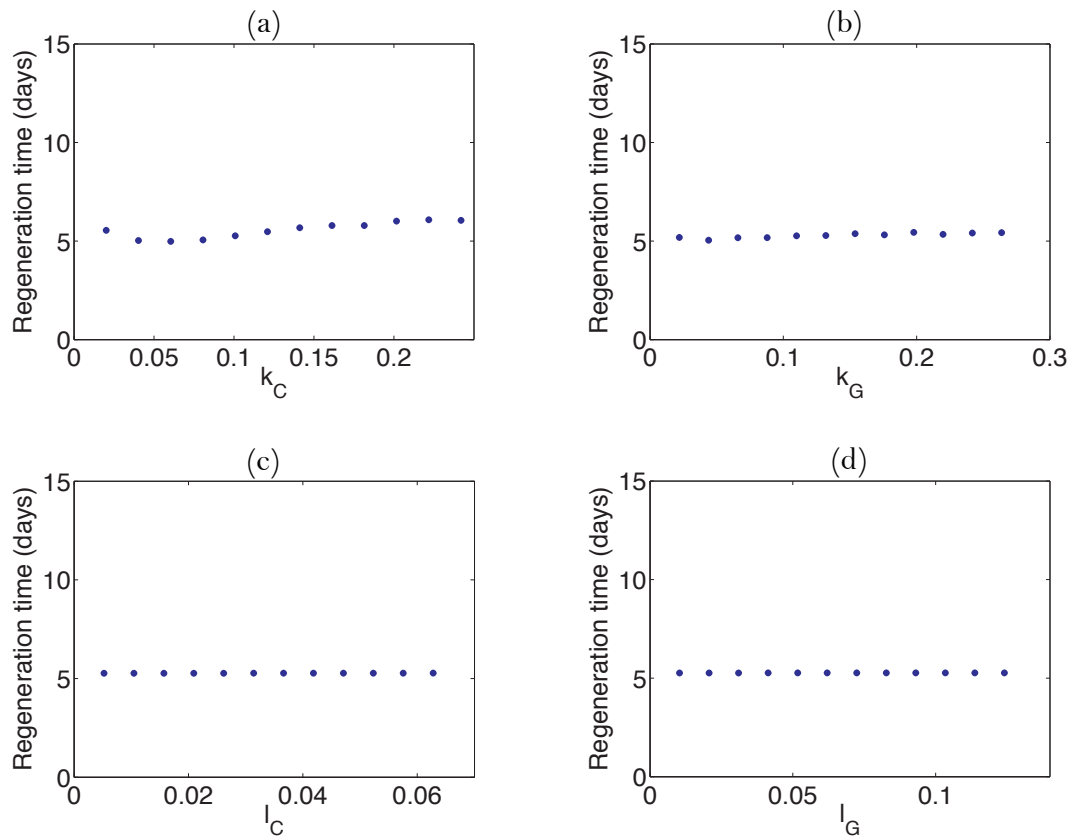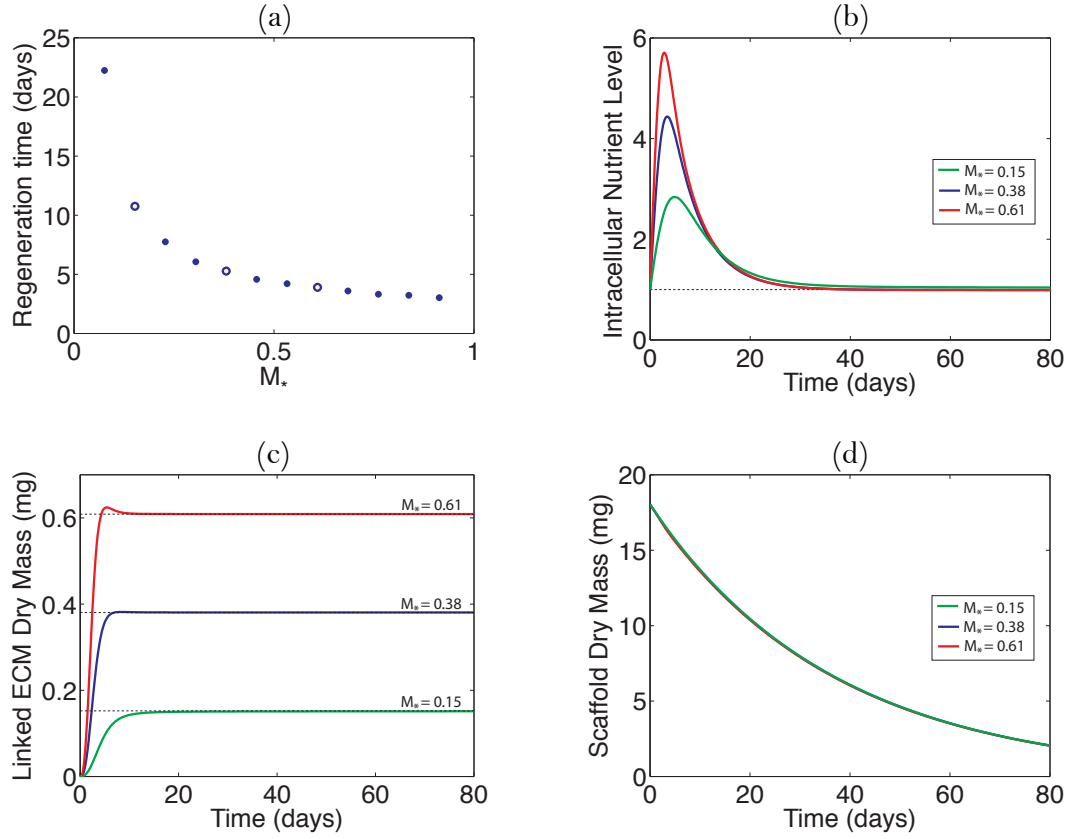Figure 4.9: (a) A plot of regeneration times for different values of d_3 found by varying the optimal parameters found previously. For the three cases denoted by the yellow/blue circles ($d_3 = 0.007$ s^{-1}, $d_3 = 0.034$ s^{-1}, and $d_3 = 0.060$ s^{-1}) plots of (b) intracellular nutrient level, (c) total linked ECM dry mass, and (d) scaffold dry mass are shown.
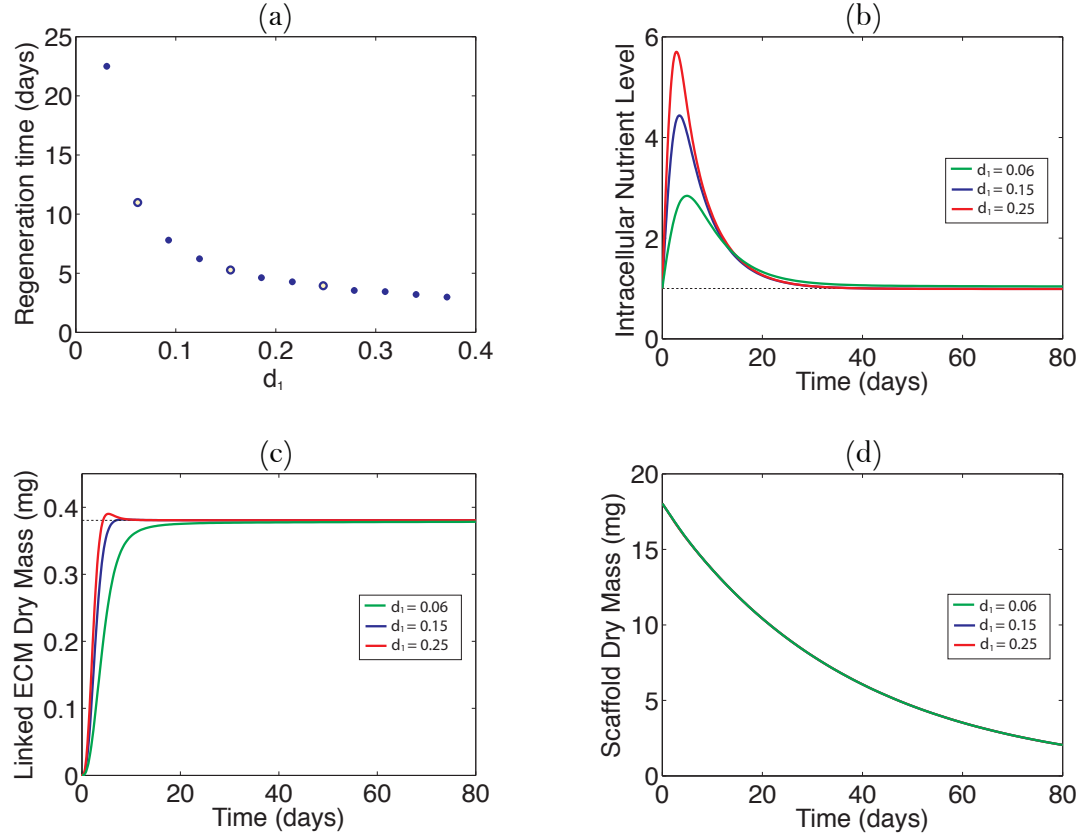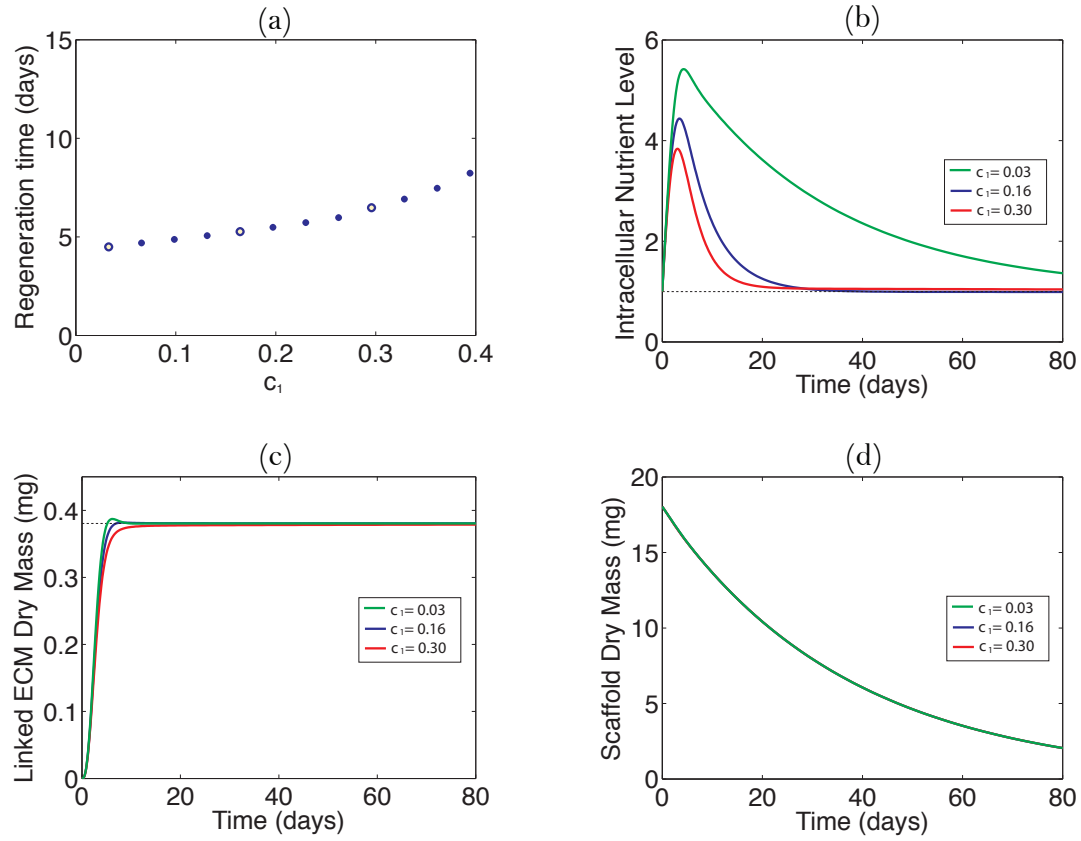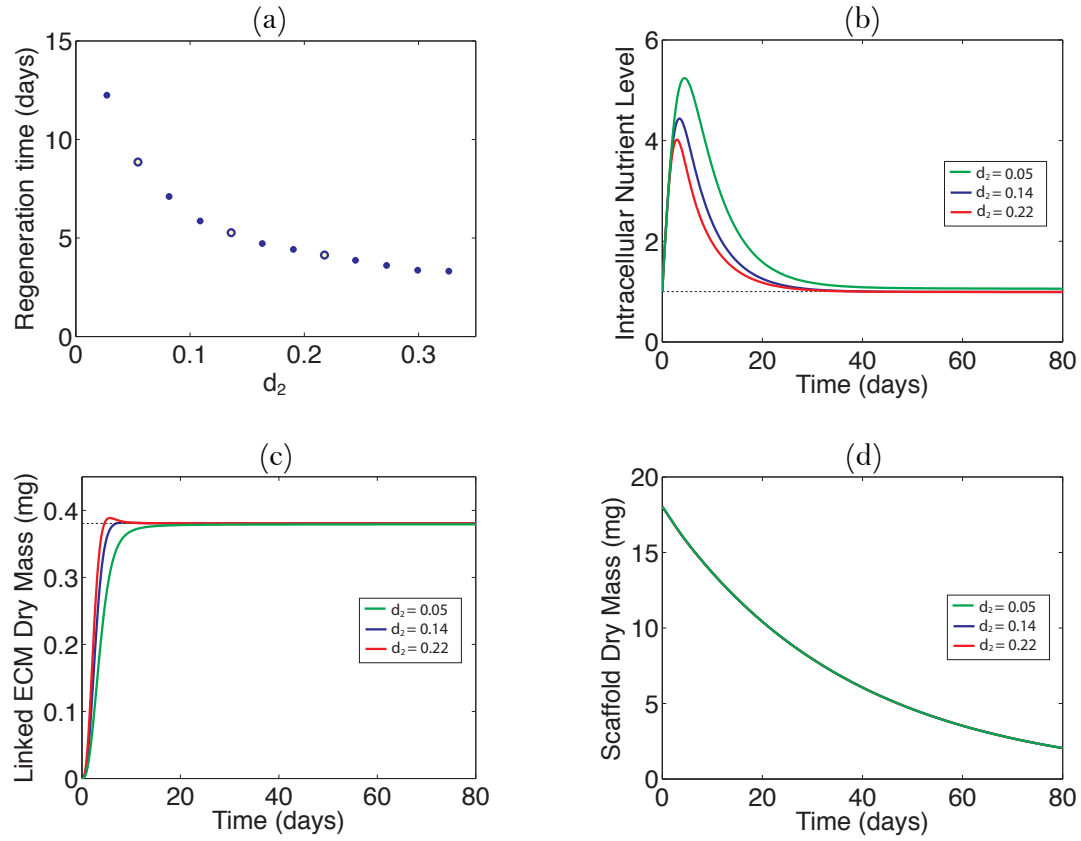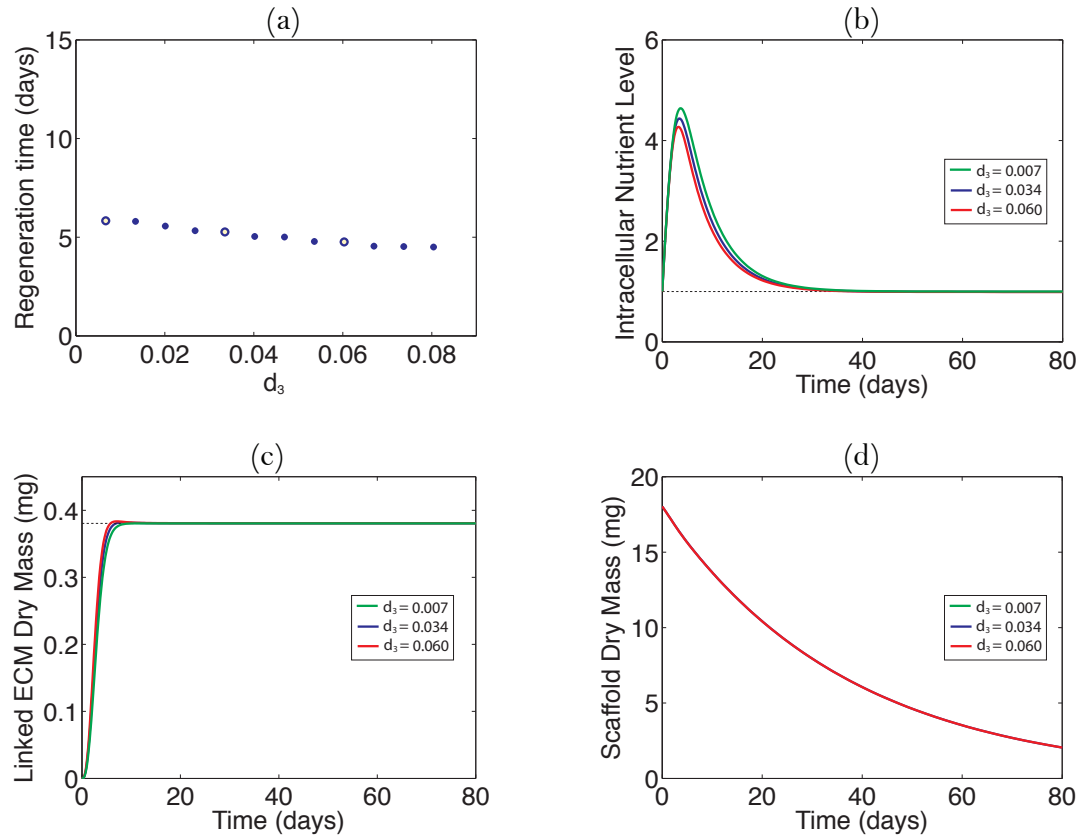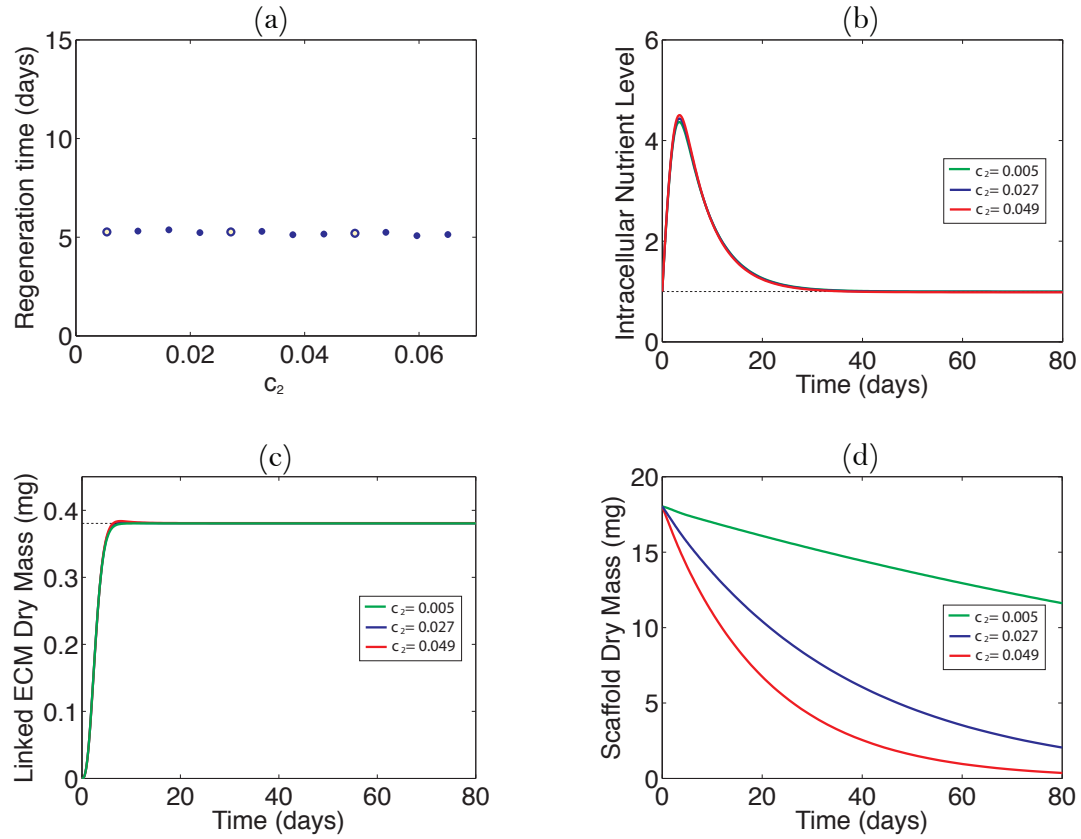
Figure 4.10: (a) A plot of regeneration times for different values of c_2 found by varying the optimal parameters found previously. For the three cases denoted by the yellow/blue circles ($c_2 = 0.005$ s^{-1}, $c_2 = 0.027$ s^{-1}, and $c_2 = 0.049$ s^{-1}) plots of (b) intracellular nutrient level, (c) total linked ECM dry mass, and (d) scaffold dry mass are shown.

4.5 Discussion

In experiments associated with cartilage tissue engineering, obtaining spatial experimental data sets at multiple time points over the course of several days or weeks can be a formidable task. As a result, spatial model results are typically spatially averaged in order to validate against data that is predominantly temporal. In this chapter, the use of an exclusively temporal model was analyzed as an efficient and potentially beneficial alternate modeling approach. The phenomenological ODE model presented here has extended the work of Wilson et al. [38] to delineate between unlinked (diffusing) and linked (bound) ECM. The Wilson et al. model was based on highly simplified assumptions about the underlying mechanisms controlling the cartilage regeneration process, but research has shown that the mechanisms at play are more complex.

Rice et al. [29] claimed that the rate and integrity of the regenerated tissue depends on the rate of hydrogel degradation: if the scaffold degrades too quickly, defects could appear, while if it degrades too slowly it could inhibit tissue growth by preventing timely distribution of the ECM molecules. The Wilson et al. model was a fully uncoupled system that did not capture the effects of product inhibition in the scaffold, and thus was explored in this current model. Obradovic et al. [24] observed that matrix synthesis depends on both the availability of nutrients and some regulatory feedback mechanism. Wilson et al. neglected the presence of nutrients entirely, but intracellular nutrient availability was included in the new model, although no experimental data was available for comparison.

The model developed in this chapter was also designed to capture the binding and linking interactions between unlinked collagen, linked collagen, and the scaffold (and similarly for GAG). After calibrating the model to the Wilson et al. data set, a parametric analysis was performed to explore the effect each parameter had on the overall cartilage regeneration time. While this modeling approach has the advantages of fast numerical computation times and availability of data, the lack of spatially-meaningful parameters could prove to be limiting. In the data set, the scaffold mass

made up a large percentage of the total construct mass, and some of the matrix-related mechanisms failed to be captured accurately as a result. Rescaling the model or changing the weights in the cost function could potentially reduce the influence of the scaffold and yield better fits. Additional mechanisms for scaffold degradation could also be explored, as the model didn't fully capture some of the data.

Chapter 5

Conclusions

In the preceding chapters, two approaches for modeling cartilage regeneration in cell-seeded scaffold materials were explored. In Chapters 2 and 3, a spatio-temporal PDE model was developed to model tissue regeneration in the local environment of a single chondrocyte seeded in a nutrient-rich hydrogel scaffold material. Recall that this model captured the interactions among extracellular matrix (ECM) synthesis, accumulation, and diffusive transport phenomena in a manner that also accounted for cell shape and the ratio of initial cell to scaffold volume. It was assumed that this process is radially symmetric within a spherical domain, and the ECM was synthesized, diffused, and accumulated uniformly around the periphery of the chondrocyte. The unlinked matrix was synthesized inside the cell and diffused freely until it bound with the scaffold, eventually replacing the hydrogel. The process by which the synthesized matrix interacted with hydrogel to form linked ECM was represented as an advancing interfacial region representing the evolving boundary between the newly formed linked ECM domain and the degrading hydrogel region. Level set and phase field modeling techniques were employed to capture the motion of this advancing region.

An advantage of this modeling approach is its formulation in terms of physically meaningful parameters, many of which can be determined from associated experiments. For example, mechanisms such as diffusion were modeled explicitly, and

diffusivities for various solute types and sizes are known or can be measured [15, 16]. Structural properties of cartilage ECM vary spatially, and this approach accounted for spatial variability in hydrogel scaffold density and degradation, and the associated changes in diffusivities through the scaffold and regenerated ECM. A parametric analysis was also performed, focusing on the dependence of ECM regeneration times on model parameters. The model proved able to capture many of the important biophysical, physiological, and scaffold-design aspects of cartilage regeneration. In the context of hydrogel scaffolds seeded with chondrocytes, this modeling approach can provide a framework for quantitative characterization of hydrogel biomaterial design. This is important because the associated experiments can be costly and time-intensive; using mathematical models could streamline the hydrogel-design process, making it more effective and efficient.

This approach is not without limitations, however. For example, numerical computations are intensive. Each simulation in Chapter 3 took on the order of hours to complete, making the full parametric analysis and power law fitting quite time-intensive. Another challenge in the application of this type of model is the difficulty in obtaining spatial data in cell-biomaterial systems. Cartilage regeneration occurs on time scales that span many days to a few weeks to several months, and many experimentalists have measured only scalar system variables such as scaffold or collagen dry mass at a small number of time points. Spatial models are typically averaged in order to validate against this data, which seems to ignore much of the potential insight that could be gained by spatial modeling.

In Chapter 4, a second approach was used to develop a phenomenological ODE model that extended previous work by Wilson et al. [38]. Since, as mentioned earlier, experimental data tends to be purely temporal, development of a simplified temporal model could prove to be both efficient and sufficiently accurate. The model presented here delineated the ECM into its collagen and GAG constituents, and the linked (bound) and unlinked (diffusing) components of each. It has been shown that the rate and integrity of the regenerated tissue depends on the rate of hydrogel degradation [29]. It has also been observed that matrix synthesis depends on both the availability

of nutrients and some regulatory feedback mechanism [24]. The model was developed to capture all of these effects, as well as the binding and linking interactions between unlinked collagen, linked collagen, and the scaffold (and similarly for GAG).

The ODE model was calibrated against the Wilson et al. data set [38], and a parametric analysis similar to the one in Chapter 3 was performed to explore the effect of each parameter on the overall cartilage regeneration time. While this modeling approach holds the advantages of very fast numerical computation times and availability of data, the lack of spatially-meaningful parameters could prove to be limiting. The model failed to effectively describe certain matrix-related mechanisms. Approaches such as employing a new cost function or rescaling the model could allow these aspects to be captured. The model didn't fully capture the scaffold degradation, and additional degradation mechanisms could also be explored.

For both approaches, the models could be extended by employing Michaelis-Menten kinetics to model nutrient consumption, as has been done by Obradovic et al. [24]. Also, since nutrient diffusion was shown to occur on a very fast time scale during analysis of the PDE model, it could reasonably be neglected in favor of a constant nutrient profile with little effect on the overall ECM regeneration time. While this could be carried over to the ODE approach, it is noted that the ODE model provides a simulation of the intracellular nutrient level through the competition between nutrient mobilization from the extracellular environment and nutrient utilization for biosynthesis of ECM constituents. Another possible simplification for the PDE model would be to treat the chondrocyte as a "black box". It could be represented as a boundary condition, described by an ODE, rather than a set of reaction-diffusion equations over an entire spatial region. Diffusivities within cells and other intracellular behavior are not well-understood and are difficult to measure, so this simplification could significantly decrease numerical computation time.

Future extensions could separate the unlinked matrix in the PDE model into its collagen and GAG constituents, as was done for the ODE model in Chapter 4. Both models could potentially be improved by explicitly modeling the presence of growth factors [36, 28]. Since the ODE model fit reasonably well to experimental data, in

future work the PDE model could be spatially averaged to compare with the ODE model and similar data sets. The available data is constraining, however, since each lab measures different quantities in a multitude of different units, and the number of data points is very small. For example, the Wilson et al. data was the only set studied here that reported scaffold mass, although some other groups did report ECM in units of percent dry mass.

As more data becomes available, the models could be calibrated and then used to predict performance of new hydrogel scaffolds. While computationally intensive, the PDE model could predict regeneration times and characteristics of the resulting cartilage on a time scale that remains significantly more efficient than the trial and error process of iterating and refining experiments. In particular, a full parametric study for specific material parameters could take anywhere from a few hours to a few days, but this is considerably faster than the several weeks or months it takes to physically regenerate articular cartilage in cell-seeded scaffolds.

Bibliography

[1] M.B. Albro, N.O. Chahine, M. Caligaris, V.I. Wei, M. Likhitpanichkul, K.W. Ng, C.T. Hung, and G.A. Ateshian, *Osmotic loading of spherical gels: a biomimetic study of hindered transport in the cell protoplasm*, Journal of Biomechanical Engineering **129** (2007), 503.

[2] G.A. Ateshian, K.D. Costa, E.U. Azeloglu, B. Morrison III, and C.T. Hung, *Continuum modeling of biological tissue growth by cell division, and alteration of intracellular osmolytes and extracellular fixed charge density*, Journal of Biomechanical Engineering **131** (2009), 101001.

[3] N.M. Bachrach, W.B. Valhmu, E. Stazzone, A. Ratcliffe, W.M. Lai, and V.C. Mow, *Changes in proteoglycan synthesis of chondrocytes in articular cartilage are associated with the time-dependent changes in their mechanical environment*, Journal of Biomechanics **28** (1995), no. 12, 1561–1569.

[4] J.A. Buckwalter and N.E. Lane, *Athletics and osteoarthritis*, The American Journal of Sports Medicine **25** (1997), no. 6, 873.

[5] M.D. Buschmann, Y.A. Gluzband, A.J. Grodzinsky, J.H. Kimura, and E.B. Hunziker, *Chondrocytes in agarose culture synthesize a mechanically functional extracellular matrix*, Journal of Orthopaedic Research **10** (1992), no. 6, 745–758.

[6] M.A. DiMicco and R.L. Sah, *Dependence of cartilage matrix composition on biosynthesis, diffusion, and reaction*, Transport in Porous Media **50** (2003), no. 1, 57–73.

[7] C.J. Galban and B.R. Locke, *Analysis of cell growth in a polymer scaffold using a moving boundary approach*, Biotechnology and Bioengineering **56** (1997), no. 4, 422–432.

[8] ———, *Analysis of cell growth kinetics and substrate diffusion in a polymer scaffold*, Biotechnology and Bioengineering **65** (1999), no. 2, 121–132.

[9] ———, *Effects of spatial variation of cells and nutrient and product concentrations coupled with product inhibition on cell growth in a polymer scaffold*, Biotechnology and Bioengineering **64** (1999), no. 6, 633–643.

[10] F. Guilak and V.C. Mow, *The mechanical environment of the chondrocyte: a biphasic finite element model of cell-matrix interactions in articular cartilage*, Journal of Biomechanics **33** (2000), no. 12, 1663–1673.

[11] S. Handley and DA Lowther, *Extracellular matrix metabolism by chondrocytes iii. modulation of proteoglycan synthesis by extracellular levels of proteoglycan in cartilage cells in culture*, Biochimica et Biophysica Acta (BBA)-General Subjects **500** (1977), no. 1, 132–139.

[12] D.W. Hutmacher, *Scaffolds in tissue engineering bone and cartilage*, Biomaterials **21** (2000), no. 24, 2529–2543.

[13] J. Kisiday, M. Jin, B. Kurz, H. Hung, C. Semino, S. Zhang, and A.J. Grodzinsky, *Self-assembling peptide hydrogel fosters chondrocyte extracellular matrix production and cell division: implications for cartilage tissue repair*, Proceedings of the National Academy of Sciences of the United States of America **99** (2002), no. 15, 9996.

[14] S.S. Kohles, C.G. Wilson, and L.J. Bonassar, *A mechanical composite spheres analysis of engineered cartilage dynamics*, Journal of Biomechanical Engineering **129** (2007), 473.

[15] H.A. Leddy, H.A. Awad, and F. Guilak, *Molecular diffusion in tissue-engineered cartilage constructs: Effects of time and culture conditions*, Journal of Biomedical Materials Research Part B: Applied Biomaterials **70B** (2004), no. 2, 397–406.

[16] H.A. Leddy and F. Guilak, *Site-specific molecular diffusion in articular cartilage measured using fluorescence recovery after photobleaching*, Annals of Biomedical Engineering **31** (2003), no. 7, 753–760.

[17] J.A. Martin and J.A. Buckwalter, *Aging, articular cartilage chondrocyte senescence and osteoarthritis*, Biogerontology **3** (2002), no. 5, 257–264.

[18] R.L. Mauck, M.A. Soltz, C.C.B. Wang, D.D. Wong, P.H.G. Chao, W.B. Valhmu, C.T. Hung, and G.A. Ateshian, *Functional tissue engineering of articular cartilage through dynamic loading of chondrocyte-seeded agarose gels*, Journal of Biomechanical Engineering **122** (2000), 252–260.

[19] V.C. Mow, C.C. Wang, and C.T. Hung, *The extracellular matrix, interstitial fluid and ions as a mechanical signal transducer in articular cartilage*, Osteoarthritis and Cartilage **7** (1999), no. 1, 41–58.

[20] J.A. Nelder and R. Mead, *A simplex method for function minimization*, The Computer Journal **7** (1965), no. 4, 308–313.

[21] D.L. Nettles, K. Kitaoka, N.A. Hanson, C.M. Flahiff, B.A. Mata, E.W. Hsu, A. Chilkoti, and L.A. Setton, *In situ crosslinking elastin-like polypeptide gels for application to articular cartilage repair in a goat osteochondral defect model*, Tissue Engineering Part A **14** (2008), no. 7, 1133–1140.

[22] D.L. Nettles, T.P. Vail, M.T. Morgan, M.W. Grinstaff, and L.A. Setton, *Photocrosslinkable hyaluronan as a scaffold for articular cartilage repair*, Annals of Biomedical Engineering **32** (2004), no. 3, 391–397.

[23] N.I. Nikolaev, B. Obradovic, H.K. Versteeg, G. Lemon, and D.J. Williams, *A validated model of gag deposition, cell distribution, and growth of tissue engineered*

cartilage cultured in a rotating bioreactor, Biotechnology and Bioengineering **105** (2009), no. 4, 842–853.

[24] B. Obradovic, J.H. Meldon, L.E. Freed, and G. Vunjak-Novakovic, *Glycosamino-glycan deposition in engineered cartilage: experiments and mathematical model*, AIChE Journal **46** (2000), no. 9, 1860–1871.

[25] S.W. O'Driscoll, *Current concepts review-the healing and regeneration of articular cartilage*, The Journal of Bone and Joint Surgery **80** (1998), no. 12, 1795–1812.

[26] S. Osher and R.P. Fedkiw, *Level set methods and dynamic implicit surfaces*, Springer Verlag, 2003.

[27] M. Pisu, N. Lai, A. Concas, and G. Cao, *A novel simulation model for engineered cartilage growth in static systems*, Tissue Engineering **12** (2006), no. 8, 2311–2320.

[28] F. Redini, P. Galera, A. Mauviel, G. Loyau, and J.P. Pujol, *Transforming growth factor [beta] stimulates collagen and glycosaminoglycan biosynthesis in cultured rabbit articular chondrocytes*, FEBs Letters **234** (1988), no. 1, 172–175.

[29] M.A. Rice and K.S. Anseth, *Controlling cartilaginous matrix evolution in hydrogels with degradation triggered by exogenous addition of an enzyme*, Tissue Engineering **13** (2007), no. 4, 683–691.

[30] A.K. Saha, J. Mazumdar, and S.S. Kohles, *Prediction of growth factor effects on engineered cartilage composition using deterministic and stochastic modeling*, Annals of Biomedical Engineering **32** (2004), no. 6, 871–879.

[31] B.G. Sengers, H.K. Heywood, D.A. Lee, C.W.J. Oomens, and D.L. Bader, *Nutrient utilization by bovine articular chondrocytes: a combined experimental and theoretical approach*, Journal of Biomechanical Engineering **127** (2005), 758–766.

[32] B.G. Sengers, M. Taylor, C.P. Please, and R.O.C. Oreffo, *Computational modelling of cell spreading and tissue regeneration in porous scaffolds*, Biomaterials **28** (2007), no. 10, 1926–1940.

[33] R.A. Stockwell, *Biology of cartilage cells*, Cambridge Univ Pr, 1979.

[34] J.S. Temenoff and A.G. Mikos, *Review: tissue engineering for regeneration of articular cartilage*, Biomaterials **21** (2000), no. 5, 431–440.

[35] A.J. Trewenack, C.P. Please, and K.A. Landman, *A continuum model for the development of tissue-engineered cartilage around a chondrocyte*, Mathematical Medicine and Biology **26** (2009), no. 3, 241–262.

[36] P.M. Van der Kraan, P. Buma, T. Van Kuppevelt, and WB Van den Berg, *Interaction of chondrocytes, extracellular matrix and growth factors: relevance for articular cartilage tissue engineering*, Osteoarthritis and Cartilage **10** (2002), no. 8, 631–637.

[37] G. Vunjak-Novakovic, B. Obradovic, I. Martin, P.M. Bursac, R. Langer, and L.E. Freed, *Dynamic cell seeding of polymer scaffolds for cartilage tissue engineering*, Biotechnology Progress **14** (1998), no. 2, 193–202.

[38] C.G. Wilson, L.J. Bonassar, and S.S. Kohles, *Modeling the dynamic composition of engineered cartilage*, Archives of Biochemistry and Biophysics **408** (2002), no. 2, 246 – 254.